RO4929097, a Selective γ-Secretase Inhibitor, Inhibits Subretinal Fibrosis Via Suppressing Notch and ERK1/2 Signaling in Laser-Induced Mouse Model

Chaoyang Zhang,[1,2] Shiyue Qin,[3] Hai Xie,[1,2] Qinghua Qiu,[1,2,4] Haiyan Wang,[1,2] Jingting Zhang,[1,2] Dawei Luo,[1,2,*] and Jingfa Zhang[1,2,*]

[1]Department of Ophthalmology, Shanghai General Hospital (Shanghai First People's Hospital), Shanghai Jiao Tong University School of Medicine, Shanghai, China
[2]National Clinical Research Center for Eye Diseases, Shanghai Key Laboratory of Ocular Fundus Diseases, Shanghai Engineering Center for Visual Science and Photomedicine, Shanghai Engineering Center for Precise Diagnosis and Treatment of Eye Diseases, Shanghai, China
[3]Department of Ophthalmology, Second Affiliated Hospital of Soochow University, Suzhou, China
[4]Department of Ophthalmology, Shigatse People's Hospital, Xizang, China

Correspondence: Dawei Luo. Department of Ophthalmology, Shanghai General Hospital (Shanghai First People's Hospital), Shanghai Jiao Tong University School of Medicine, 100 Haining Road, Hongkou District, Shanghai 200080, China; dr-davie@yeah.net.
Jingfa Zhang, Department of Ophthalmology, Shanghai General Hospital (Shanghai First People's Hospital), Shanghai Jiao Tong University School of Medicine, 100 Haining Road, Hongkou District, Shanghai 200080, China; 13917311571@139.com.

DL and JZ are co-corresponding author and they contributed equally to this work.

Received: March 28, 2022
Accepted: August 30, 2022
Published: September 26, 2022

Citation: Zhang C, Qin S, Xie H, et al. RO4929097, a selective γ-secretase inhibitor, inhibits subretinal fibrosis via suppressing notch and ERK1/2 signaling in laser-induced mouse model. *Invest Ophthalmol Vis Sci.* 2022;63(10):14. https://doi.org/10.1167/iovs.63.10.14

Purpose. This study aimed to explore whether RO4929097 (RO), a specific γ-secretase inhibitor, could inhibit the subretinal fibrosis in laser-induced mouse model and the relevant molecular mechanisms.

Methods. Male C57BL/6J mice were used to produce choroidal neovascularization (CNV) and subretinal fibrosis by laser photocoagulation, and RO was administered intravitreally 1 day after laser induction. The sizes of CNV and subretinal fibrosis were measured and quantified in both 2D and 3D constructions. The ARPE-19 cell line and primary human RPE (phRPE) cells were treated with TGFβ1, in combination with or without RO, to examine Notch related molecules, epithelial mesenchymal transition (EMT), cell viability, migration, and contractile function, as well as the crosstalk between Notch and other EMT relevant signaling pathways.

Results. Intravitreal injection of RO reduced the sizes of both CNV and subretinal fibrosis in laser-induced young and old mice at day 7 and day 14 after laser induction. Moreover, EMT and Notch activation in RPE-choroid complexes from laser-induced mice were significantly attenuated by RO. In vitro, TGFβ1 activated Notch signaling and induced EMT in ARPE-19 cells, accompanied by enhanced EMT-related function, which were inhibited by RO. The inhibition of RO on EMT was further confirmed in TGFβ1-treated phRPE cells. Blockage of Notch signaling by RO could inhibit ERK1/2 signaling; whereas ERK1/2 inhibition had no effect on Notch. The action of RO was independent of Smad2/3 or p38, and co-inhibition of Notch and Smad2/3 showed synergistic effect on EMT inhibition.

Conclusions. RO exerts its antifibrotic effect by directly inhibiting Notch signaling and indirectly suppressing ERK1/2 signaling. Targeting Notch signaling might provide a therapeutic strategy in prevention and treatment of subretinal fibrosis in neovascular age-related macular degeneration (nAMD).

Keywords: neovascular age-related macular degeneration (nAMD), choroidal neovascularization (CNV), subretinal fibrosis, Notch, transforming growth factor β, retinal pigment epithelium (RPE)

Age-related macular degeneration (AMD) is the leading cause of severe visual impairment and blindness among the elderly worldwide, which is predicted to rise to 288 million by the year 2040.[1] Its wet form, also called neovascular AMD (nAMD), leads to irreversible central vision loss caused by choroidal neovascularization (CNV), and ultimately develops into a permanent subretinal fibrovascular scar.[2] Anti-vascular endothelial growth factor (anti-VEGF) agents have become the first-line therapy for nAMD treatment, which could inhibit CNV and decrease retinal leakage evidently.[3–5] However, a substantial portion of patients (around one-third) still develop subretinal fibrosis (or macular fibrosis) even with intensive anti-VEGF treatment,[6] resulting in poor visual prognosis and proposing a huge challenge in nAMD treatment.

Subretinal fibrosis contains vascular and fibrotic components, also known as fibrovascular scar, but it is still unclear how the abnormal vessels transformed into a fibrovascular tissue.[7,8] The main characteristic of subretinal fibrosis is the excess of extracellular matrix (ECM)

proteins, such as collagens and fibronectin, which originated from multiple cell types, including transdifferentiated retinal pigment epithelium (RPE), activated Müller glia, endothelial cells, microglia, pericytes, myofibroblast-like cells, etc.[9–11] RPE cells maintain the retinal homeostasis under normal conditions. However, in some pathological conditions, RPE cells differentiate into myofibroblast-like cells by epithelial-mesenchymal transition (EMT), contributing to ECM deposition and fibrosis formation.[12] Increasing evidence suggested that transdifferentiated RPE cells were involved in the formation and development of the fibrosis in nAMD, inherited retinal degenerations (IRDs), proliferative diabetic retinopathy (PDR), and proliferative vitreoretinopathy (PVR), etc.[10,11,13,14] Because CNV tissues from both patients with nAMD and laser-induced CNV mice showed the significant contribution of TGF-β/Smad signaling pathway involving the EMT of RPE cells during the development of subretinal fibrosis,[15,16] laser-induced CNV mice were widely used as the experimental animal model to study EMT-mediated subretinal fibrosis in nAMD.[11,17–19]

The Notch signaling is a highly conserved molecular mechanism of intercellular interaction (i.e. responsible for the regulation of cell differentiation, proliferation, apoptosis, and stem cell maintenance),[20] which also controls fibrosis in some organs.[16,21–23] Binding of Notch ligands (Jagged1, Jagged2, and Delta-like1, 3 and 4) with its receptors (Notch1-4) leads to the activation of γ-secretase proteases, which results in the proteolytic cleavage of the Notch intracellular domain (NICD). The cleaved NICD translocates to the cell nucleus and acts as a transcriptional activator to activate transcription of downstream genes, including those involved in fibrosis.[24,25] The γ-secretase is a multiprotein complex comprised of 4 integral membrane proteins (i.e. nicastrin, presenilin [1 and 2], presenilin enhancer 2 [PEN2], and anterior pharynx defective 1). Stoichiometric assembly of these four components is essential for the normal function of the whole complex; whereas the loss of any subunit leads to the retention of other subunits in the endoplasmic reticulum or fast degradation.[26] It was reported that blockage of NICD cleavage with a γ-secretase inhibitor (GSI) could downregulate the downstream target genes of Notch signaling.[27] Moreover, the activation of Notch signaling has been revealed to contribute to EMT in TGFβ-treated ARPE-19 cells and PVR formation in mouse model, which could be reversed by LY411575 or DAPT (two specific GSIs).[28,29] These results suggested that Notch signaling plays an important role in fibrosis formation mediated by RPE through EMT. In laser-induced CNV rodent models, intravitreal injection of DAPT at a low concentration (16 ng/eye) showed no evident effect on the volume of CNV lesion,[30] however, the angiogenesis was aggravated if a high dosage (200 µg/eye) was used.[31] Currently, there is no research about the effect of GSIs on subretinal fibrosis in laser-induced CNV mice.

It was reported that RO4929097 (RO), one specific GSI, showed higher efficiency in Notch inhibition than DAPT.[32] In addition, RO has been revealed to prevent retinal fibrosis in the sodium iodate induced mouse model by targeting Müller glia.[33] However, it remains unclear that whether or not RO could prevent subretinal fibrosis and EMT in a laser-induced CNV model. Here, we studied the effect of RO on subretinal fibrosis and EMT both in the laser-induced CNV mouse model and TGFβ1-treated RPE cells. We also investigated the crosstalk between Notch and other EMT related signaling pathways, including canonical TGFβ/Smad signaling and MAPKs. The data showed that Notch signaling was activated both in vivo and in vitro, participating in subretinal fibrosis and EMT, which was significantly reversed by RO. Notch might be the upstream signaling of ERK1/2, and combined inhibition of Notch and Smad2/3 showed a synergistic effect on EMT inhibition. Thus, targeting Notch signaling by RO or other inhibitors might provide an alternative therapeutic strategy in prevention and treatment of subretinal fibrosis in nAMD and other fibrovascular diseases.

Materials and Methods

Reagents and Antibodies

The specific inhibitors, including RO4929097 (RO; S1575), DAPT (S2215), U0126-EtOH (S1102), SB431542 (S1067), and Adezmapimod (S1076) were purchased from Selleck (Shanghai, China). Recombinant TGFβ1 (PHG9214) was purchased from ThermoFisher (Shanghai, China). DMEM/F12 medium (11330-032) was purchased from HyClone (Logan, UT, USA). Fetal bovine serum (FBS; 40130ES76), Penicillin/streptomycin (60162ES76), RIPA lysis buffer (20101ES60), Bicinchoninic Acid (BCA) Protein Quantification Kit (20201ES76), methylthiazolyldiphenyltetrazolium bromide (MTT; 40201ES72) and Crystal Violet Stain Solution (0.5%; 60506ES60) were purchased from Shanghai Yeasen Biotechnology Co. Ltd. (Shanghai, China). The antibody information is listed in Table 1.

Laser-Induced CNV Model and Animal Treatment

The mouse CNV model was established with laser photocoagulation according to the previously published method.[34] Seven-week-old (young) and 13-month-old (old) C57BL/6J male mice were purchased from Shanghai SLAC Laboratory Animal Co., Ltd. (Shanghai, China). Briefly, after anesthesia and pupil dilation, the 4 laser-induced spots (50 µm) were generated by 532-nm laser with a power of 120 mW for 100 ms (Carl Zeiss Meditec, Dublin, Ireland) in a standard fashion surrounding the optic nerve head with the help of a slip-lamp delivery system.

The stock solution of RO was dissolved in DMSO at a concentration of 10 mM. RO (1 µL; 100 µM) was administered intravitreally (CNV + RO), with the contralateral eye injected with the same volume of phosphate-buffered saline (PBS) containing 1% DMSO as a vehicle control (CNV + vehicle), followed the previous method,[35] at one day after laser induction. Three, 7, and 14 days after laser induction, RPE-Bruch's membrane choriocapillaris complex (RBCC) were isolated, according to our previous method,[36] for further examination by using Western blot, and immunofluorescence analysis was carried out in RPE-choroid-sclera complexes.

Quantification of the Sizes of CNV and Subretinal Fibrosis

The sizes of CNV and subretinal fibrosis were measured and quantified as the volume (μm^3) and area (μm^2) with the immunostaining of isolectin B4 (IB4) and collage I by using ImageJ software (1.53k; National Institutes of Health, Bethesda, MD, USA). For volume measurement of both CNV and subretinal fibrosis, confocal z-stacks of IB4 and collagen I immunofluorescence were recorded at × 20 magnification using a Leica SP8 confocal microscope (Leica, Germany). The 3D z-stack reconstruction and image export were performed

Investigative Ophthalmology & Visual Science

Table 1. Antibody Information

Target	Catalogue no.	Application (Conc.)	Vendor
Jag1	ab7771	WB (1:1,000)	Abcam
p-Smad2/3	8828	WB (1:1,000)	Cell Signaling Technology
Smad2/3	8685	WB (1:1,000)	Cell Signaling Technology
Notch1	3608	WB (1:1,000)	Cell Signaling Technology
NICD (Cleaved Notch1)	4147	WB (1:1,000)	Cell Signaling Technology
DLL4	2589	WB (1:1,000)	Cell Signaling Technology
Hes1	11988	WB (1:1,000)	Cell Signaling Technology
γ Secretase Antibody Sampler Kit	5887	WB (1:1,000)	Cell Signaling Technology
p-ERK1/2	4370	WB (1:1,000)	Cell Signaling Technology
ERK1/2	9107	WB (1:1,000)	Cell Signaling Technology
p-p38	9216	WB (1:1,000)	Cell Signaling Technology
p38	9212	WB (1:1,000)	Cell Signaling Technology
Fibronectin	15613-1-AP	WB (1:500);IF (1: 100)	Proteintech
Collagen I	ab34710	WB (1:1,000);IF (1: 100)	Abcam
α-SMA	Ab7817	WB (1:2,000);IF (1: 100)	Abcam
ZO-1	61-7300	WB (1:1,000);IF (1: 100)	Invitrogen
RPE-65	Ab13826	IF (1: 100)	Abcam
GAPDH	10494-1-AP	WB (1: 5,000)	Proteintech

WB, Western blot; IF, immunofluorescence.

with Leica LAS X software. The quantification of immunofluorescence volume was carried out by 3D Object Counter plugin of ImageJ. Briefly, after 8-bit conversion and scale bar correction, the valid fluorescence signal was included for quantification (volume and area) by setting an appropriate threshold. In order to visualize the quantification process, an example of area quantification for collagen I immunostaining with ImageJ software is shown in Supplementary Figure S1.

Cell Culture

Primary human RPE (phRPE) cells were isolated from donors' eyes (obtained from the Eye Bank of Shanghai Tenth People's Hospital, Shanghai, China), and cultures were established following the published method.[37] The current research involving human participants was approved by the Ethics Committee of Shanghai General Hospital and was in compliance with the Declaration of Helsinki. The phRPE cells at passage 2 to 4 was used in this study. A human RPE cell line (ARPE-19) was obtained from American Type Culture Collection (ATCC, Manassas, VA, USA).

The complete medium for phRPE and ARPE-19 cell culture contains DMEM/F12 medium, penicillin/streptomycin (1%), and fetal bovine serum (10%). First, RPE cells were seeded uniformly and cultured in serum-free medium for 12 hours. Then, the cells were randomly divided into three groups (i.e. the vehicle-treated group [vehicle], the TGFβ1 [10 ng/mL] + vehicle-treated group [TGFβ1 + vehicle], and the TGFβ1 + RO [10-80 µM]-treated group [TGFβ1 + RO]). Pretreatment of ARPE-19 cells with U0126 (10 µM), SB431542 (SB; 10 µM), and Adezmapimod (Ad; 10 µM), when needed, was carried out 1 hour prior to treatment with TGFβ1. TGFβ1 was reconstituted in an acidic buffer (4 mM HCl) and the inhibitors (RO, DAPT, U0126, SB431542, and Adezmapimod) were dissolved in DMSO at a concentration of 10 mM. Therefore, vehicle-treated cells (Vehicle) were incubated with culture medium containing 4 µM HCl or/and 0.1 to 0.8% DMSO, and TGFβ-treated cells (TGFβ1 + vehicle) were treated with 0.1 to 0.8% DMSO, when needed, throughout the in vitro study. After incubation for 1 to 48 hours, the cells were harvested for the following study.

Scratch Assay

ARPE-19 cells were uniformly seeded in 24-well plates (2 $\times$ 10^5 cells per well). After cell culture for 24 hours, ARPE-19 cells were deprived of serum for 12 hours before treatment of TGFβ1 (10 ng/mL) and RO (40 µM). The monolayer of ARPE-19 cells was scratched with a thin rubber tip to generate a 1 mm-wide wound. The width of the wound was measured at 0, 24, and 48 hours after scratch with a fluorescence microscope (Leica, DMI3000, Germany), and the quantification was performed by using the ImageJ software.

Transwell Migration Assay

ARPE-19 cells were uniformly seeded in 6-well plates (1 $\times$ 10^6 cells per well). After 48 hours of treatment, ARPE-19 cells were trypsinized and harvested. Then, 2 $\times$ 10^5 cells were seeded into the upper compartment of a Transwell with the pore size of 8 µm (Falcon; Corning Life Sciences, Corning, NY, USA). Then, 500 mL of complete medium was added to the outer compartment of the Transwell. After 48 hours of incubation, a swab was used to carefully remove the cells in the upper compartment of the Transwell. The Transwell membrane was fixed with cold methanol for 10 minutes, and the ARPE-19 cells were stained with Crystal Violet Stain Solution (0.5%) for 1 hour. The staining was visualized with a Leica microscope (DMI3000, Germany), and quantification (cell number) was performed with the help of ImageJ software.

Gel Contraction Assay

Collagen gel contraction assay was performed as described previously.[38] First, 24-well plates were coated with 1% bovine serum albumin (BSA) solution for 1 hour at 37°C. TGFβ1-treated ARPE-19 cells with or without RO (40 µM) for

Table 2. The Information of Human Primers

Gene	Forward (5′-3′)	Reverse (5′-3′)
Fibronectin	AAGACCATACCCGCCGAATG	GGCATTTGGATTGAGTCCCG
Collagen I	AATGTGGTTCGTGACCGTGA	AGCCTTGGTTGGGGTCAATC
α-SMA	CAGAAGGAGATCACGGCCCTAG	CGGCTTCATCGTATTCCTGTTTG
ZO-1	AGCCATTCCCGAAGGAGTTGAG	ATCACAGTGTGGTAAGCGCAGC
Transgelin	AAGCGCAGGAGCATAAGAGG	ACTGATGATCTGCCGAGGTC
MMP2	TGATGGCATCGCTCAGATCC	GGCCTCGTATACCGCATCAA
ITGA5	GGTCGGGGGCTTCAACTTA	AGCACACTGACCCCGTCTG
SNAIL1	TGCAGGACTCTAATCCAGAGTTT	GGACAGAGTCCCAGATGAGC
Hes1	CTGAGCACAGACCCAAGTGT	GAGTGCGCACCTCGGTATTA
GAPDH	CATCAGCAATGCCTCCTGCAC	TGAGTCCTTCCACGATACCAAAGTT

48 hours were harvested in serum-free DMEM/F12 medium. Collagen I from rat tail (final concentration, 2 mg/mL; Corning, 354249, Shanghai, China), 10 × DMEM/F12, RPE cell suspension (final cell density, 2.5 × 10^5 cells/well), 1 N NaOH, and sterile water were mixed on ice, and then transferred into BSA-coated wells for 1 hour at 37°C until the gel solidified. The collagen gel was subsequently freed from the wall of the well with a pipette tip carefully and another 0.5 mL of serum-free DMEM/F12 medium was added into the well. After 48 hours, digital photographs of the gels were captured and the ratio of the gel area (% from initial) was quantified using ImageJ software.

Real-Time Quantitative PCR

Isolation of total RNA and real-time quantitative PCR (RT-qPCR) were performed following our previous methods.[35] Total RNA was extracted form ARPE-19 cells with TRIeasy LS Total RNA Extraction Reagent (19201ES60; Yeasen, Shanghai, China). The cDNA Synthesis SuperMix (11120ES60, Yeasen; Shanghai, China) was used to perform reverse transcription. SYBR Green master mix (11201ES03, Yeasen; Shanghai, China) was used to conduct RT-qPCR in Bio-Rad CFX Manager 2.1 Detection system (Hercules, CA, USA). The information of human primers is listed in Table 2.

Western Blot

RIPA buffer was used to lyse the samples of mouse RBCCs and RPE cells. Protein concentration was examined with the help of BCA assay. Western blot was conducted following our previous protocol.[35] Briefly, the proteins from different groups were resolved in 7.5 to 12.5% SDS-PAGE gels, then transferred electrophoretically onto PVDF membranes. The blots were blocked for 1 hour at room temperature with 5% BSA in TBST (10 mM Tris, pH 8.0, 150 mM NaCl, 0.5% Tween 20). Then, the membranes were incubated separately with the primary antibodies against DLL4, Jag1, Nicastrin, Presenilin1, Presenilin2, PEN2, NICD, Notch1, GAPDH, Smad2/3, ERK1/2, and p38 overnight at 4°C. After thorough washing with TBST, the blots were incubated with the corresponding secondary antibodies for 1 hour at room temperature. After extensive washing with TBST, the blots were scanned by using Odyssey infra-red imaging system from LICOR Biosciences (Lincoln, NE, USA). The densitometric values for interested proteins were normalized by GAPDH, and the optical density of each band was examined with Quantity One software (Bio-Rad).

Immunofluorescence

The immunofluorescence was performed as described previously.[35] Briefly, after fixation with PBS-buffered 4% paraformaldehyde, the mouse RPE-choroid-sclera complexes and RPE cells were permeabilized and blocked in PBS containing 0.05% Triton X-100 and 1% BSA for 1 hour. Then, the samples were separately incubated with the primary antibodies against Collagen I, Fibronectin, α-SMA, RPE65, Isolectin B4 (IB4; 1:500), and ZO-1 at 4°C overnight. After thorough washing by PBS, the samples were then incubated with the corresponding secondary antibodies (1:500) for 1 hour in the dark at room temperature. The samples were mounted with coverslips and the immunostaining was visualized with a confocal microscope from Carl Zeiss (LSM 710; Königsallee, Germany).

Statistics

All experiments were repeated at least three times. All data were expressed as mean ± SEM. Statistical analysis was performed with GraphPad Prism version 8.0. Comparisons between 2 experimental groups were performed using the 2-tailed unpaired Student's *t*-test. Statistical analysis for differences among groups was tested by 1-way ANOVA with Dunnett's or Tukey's multiple comparisons test. A P value of 0.05 or less was considered statistically significant.

Results

RO Decreased the Sizes of CNV and Subretinal Fibrosis in Laser-Induced CNV Mouse Model

To examine the efficacy of RO in reducing CNV and subretinal fibrosis, immunostaining of isolectin B4 (IB4; endothelial cell marker) and ECM protein collagen type I (Collagen I) was performed in both 7-week-old (young) and 13-month-old (old) laser-induced CNV mice, because age has been reported as an independent risk factor for CNV severity.[39] As shown in Figure 1A, comparative analysis of vascular morphology of CNV lesions 7 days after laser induction showed that the CNV lesions of young mice displayed the capillary phenotype with ill-defined network of microvessels (capillary CNV), whereas the old mice displayed arteriolarized phenotype with large-caliber lumen and terminal vascular loops (ateriolar CNV). Moreover, as compared with young mice, old mice developed more severe CNV and subretinal fibrosis, as indicated by significantly larger volume and area of CNV and increased ECM deposition (Figs. 1B–E).

Investigative Ophthalmology & Visual Science

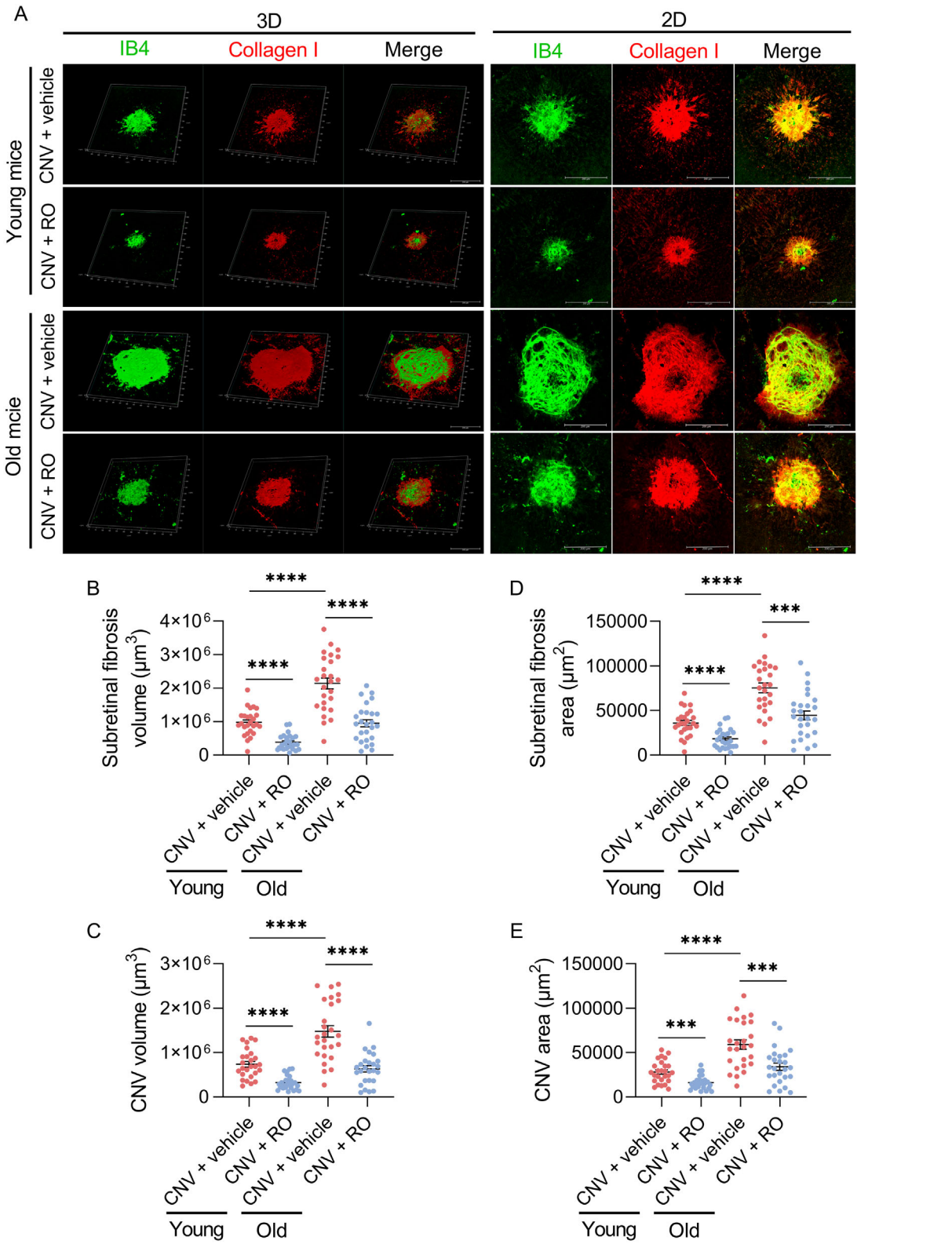

Figure 1. The effect of RO on CNV and subretinal fibrosis in laser-induced CNV mice. (**A**) Representative 3D and 2D images of IB4 and collagen I immunostaining in RPE-choroid complex flatmounts in laser-induced young mice (7 weeks old) and old mice (13 months old) with or without intravitreal RO treatment at day 7 after laser induction. Quantification of the volume of subretinal fibrosis (**B**) and CNV (**C**) as well as the area of subretinal fibrosis (**D**) and CNV (**E**) among 4 groups ($n = 26$ lesions/group). Data are expressed as mean ± SEM. *** $P < 0.001$, **** $P < 0.0001$; 2-tailed Student's t tests **B** to **E**. Scale bar = 200 μm **A**. CNV, choroidal neovascularization; RO, RO4929097; young, 7-week-old mice; old, 13-month-old mice; vehicle, 1 μL phosphate-buffered saline (PBS) containing 1% DMSO.

Investigative Ophthalmology & Visual Science

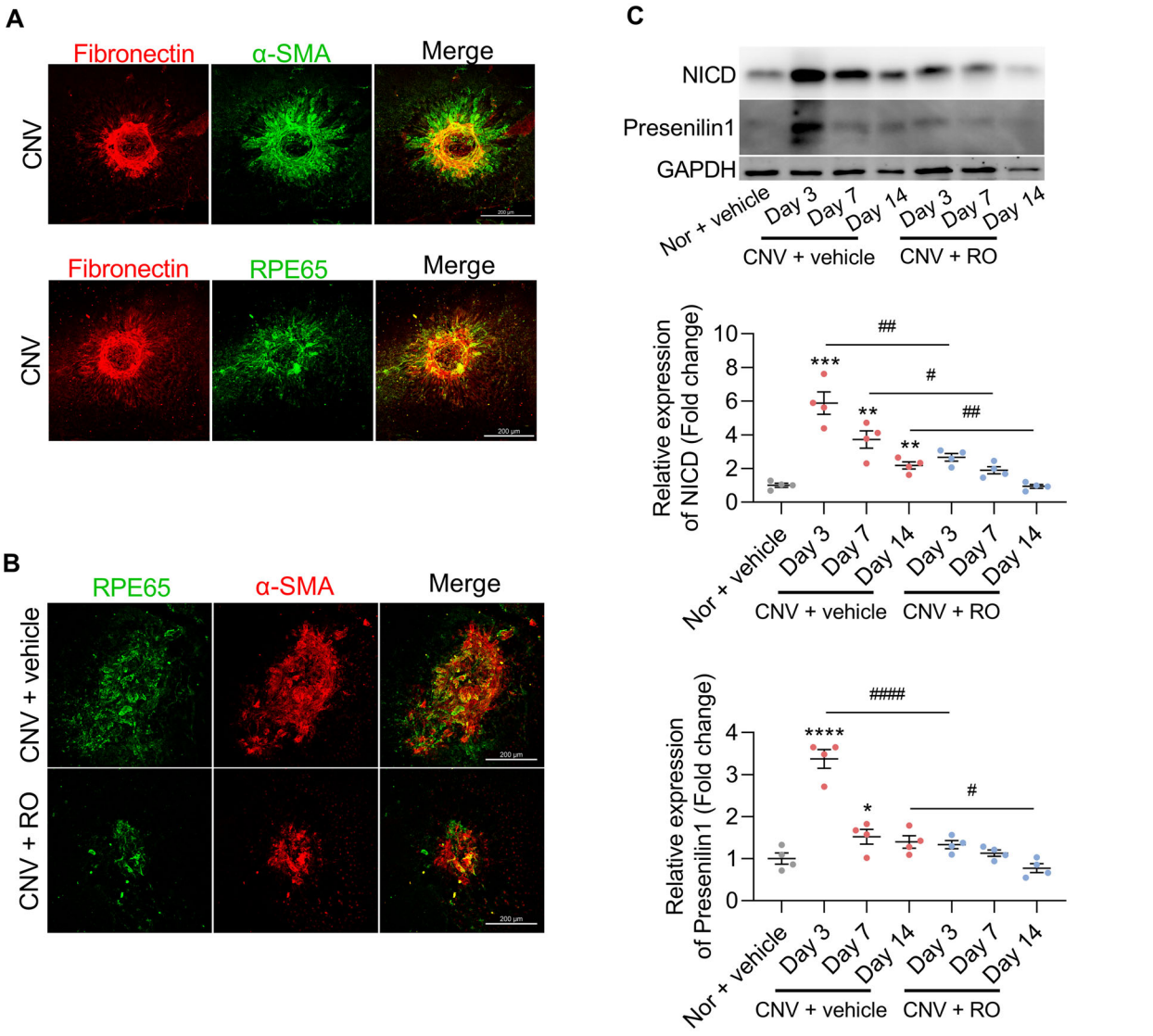

Figure 2. The effect of RO on EMT and Notch signaling in laser-induced CNV mice. (**A**) Immunostaining of fibronectin (ECM protein), α-SMA (mesenchymal marker), and RPE65 (RPE marker) in RPE-choroid complex flatmounts from laser-induced CNV mice at day 7 after laser induction. (**B**) Representative images of double immunostaining for RPE65 and α-SMA in RPE-choroid complex flatmounts from laser-induced CNV mice treated with or without RO for 7 days. (**C**) The changes of Notch related molecules (NICD and presenilin1) examined with Western blot in RBCCs from day 3 to day 14 after laser induction with or without RO treatment ($n = 4$ mice). Data are expressed as mean ± SEM. * $P < 0.05$, ** $P < 0.01$, *** $P < 0.001$, **** $P < 0.0001$; $^{\#}$ $P < 0.05$, $^{\#\#}$ $P < 0.01$, $^{\#\#\#\#}$ $P < 0.0001$; 1-way ANOVA with Tukey's multiple comparisons test **C**. Scale bar = 200 µm **A** and **B**. CNV, choroidal neovascularization; Nor, normal control; RO, RO4929097; vehicle, 1 µL PBS containing 1% DMSO.

Interestingly, the CNV and subretinal fibrosis of both young and old mice were markedly alleviated by intravitreal injection of RO. After RO treatment, the volume and area of CNV were significantly decreased by 56.34% ($P < 0.0001$; see Fig. 1C) and 42.75% ($P < 0.001$; see Fig. 1E), respectively, in laser-induced young mice (7 weeks old) when compared to those of vehicle treated mice. The same trend was also observed in the change of subretinal fibrosis, which showed a significantly reduction by 60.94% ($P < 0.0001$; see Fig. 1B) in volume and by 49.47% ($P < 0.0001$; see Fig. 1D) in area, respectively, in young CNV mice after RO treatment as compared to vehicle treated mice. Similarly, on day 14 after laser induction, the sizes of IB4 and collagen I immunostaining were significantly decreased after RO treatment in young mice (Supplementary Fig. S2). As for laser-induced old mice (13 months old), the similar results were observed when treated with RO, indicating its broad applicability for both CNV and subretinal fibrosis in laser-induced CNV mice.

RO Suppressed EMT and Notch Activation in Laser-Induced Mouse Model

Increasing evidence indicates that EMT was participated in the subretinal fibrosis secondary to CNV. Accordingly, the contribution of EMT to the subretinal fibrosis in laser-induced CNV model was confirmed. As shown in Figure 2A, the double immunostainings displayed the well colocalization of ECM protein fibronectin with α-smooth muscle actin (α-SMA; a mesenchymal marker) and RPE65 (a RPE specific

Investigative Ophthalmology & Visual Science

marker) in the mouse RPE-choroid complex flatmounts on day 7 after laser induction, indicating the involvement of transdifferentiated RPE cells in the formation of subretinal fibrosis. To further confirm this and examine the effect of RO on EMT, RO was intravitreally injected, as shown in Figure 2B, as compared with the CNV + vehicle group (7 days), the overlap area of RPE65 and α-SMA immunostaining was obviously reduced with intravitreal injection of RO 1 day after laser induction, indicating the anti-EMT effect of RO.

Furthermore, to investigate whether Notch signaling was involved in the CNV-induced subretinal fibrosis, the expressions of NICD and presenilin1 were examined. In Figure 2C, as compared with the Nor + vehicle group, the protein levels of NICD and presenilin1 were upregulated in RBCCs from the CNV + vehicle group in a time-dependent manner (i.e. the upregulation was most obviously at day 3, then decreased but still higher than that of the Nor + vehicle group), indicating the activation of Notch signaling. Moreover, the activation of Notch signaling was partially reversed by RO treatment at different time points (see Fig. 2C).

RO Attenuated the EMT in TGFβ1-Treated RPE Cells

MTT assay was used to detect the cytotoxicity of RO on ARPE-19 cells. As shown in Supplementary Figure S3, ARPE-19 cells were incubated with different concentrations of RO from 1 to 160 µM. The results demonstrated that RO, only when at 160 µM, significantly reduced the cell viability, thus the concentrations less than 160 µM were selected (10, 20, 40, and 80 µM) in the following experiments.

To validate the anti-fibrotic and anti-EMT role of RO in laser-induced CNV mice, TGFβ1-treated ARPE-19 cell line was used to determine the inhibitory effect of RO on EMT in vitro. As shown in Supplementary Figure S4A, RT-qPCR data showed that ARPE-19 cells incubated with TGFβ1 for 48 hours significantly upregulated the mRNA levels of EMT markers, including fibronectin, collagen I, α-SMA, transgelin, matrix metallopeptidase 2 (MMP2), integrin α5 (ITAG5), SNAIL1, as well as a Notch downstream effector hairy and enhancer of split 1 (Hes1), whereas significantly downregulated the epithelial marker tight junction protein ZO-1, indicating the successful establishment of the EMT cell model. Consistently, significant decrease of ZO-1 mRNA level and increase of fibronectin, collagen I, and α-SMA expressions were observed in TGFβ1-treated ARPE-19 cells for 48 hours, which were evidently reversed by co-incubation of RO dose-dependently (Figs. 3A–D). Moreover, RO also showed the similar effect on the expressions of transgelin, MMP2, and SNAIL1 by using RT-qPCR (see Supplementary Fig. S4B–D). The above changes were further confirmed by Western blot and immunofluorescence (i.e. upregulation of EMT markers [fibronectin, collagen I, and α-SMA] and disruption of ZO-1 in TGFβ1 treatment group were evidently reversed by RO treatment; Figs. 3E, 3F). In addition, bright field images demonstrated the myofibroblast-like morphology, with a spindle shape, in TGFβ1-treated ARPE-19 cells was largely reversed by RO treatment (see Fig. 3F). These above data indicated that RO was able to inhibit the EMT in TGFβ1-treated ARPE-19 cells.

To further substantiate the above observations in a polarized RPE cells with greater fidelity mimicking its in vivo situation, phRPE cells were used. As shown in Figure 4A, after isolation and culture of phRPE, large amounts of intracellular pigments were clearly observed. These RPE cells were further identified by the positive immunostaining of RPE65 in cytoplasm (Fig. 4B). Then, the role of RO in regulating EMT was verified in TGFβ1-treated phRPE cells by using Western blot and immunofluorescence. Similar to the results in ARPE-19 cells (see Fig. 3), EMT inhibition by RO in TGFβ1-treated phRPE was evidenced by the downregulation of EMT-related proteins (fibronectin, collagen I, and α-SMA) and upregulation of the epithelial marker E-cadherin (no expression in ARPE-19 cells; Fig. 4C). The Western blot results were further substantiated by the immunofluorescence (Fig. 4D). Confocal z-stacks of ZO-1 immunostaining demonstrated the characteristic of RPE polarity and more complete tight junction than ARPE-19 cell line. Although the TGFβ1-induced decrease of content of ZO-1 protein showed no significant change with addition of RO (see Fig. 4C), disorganization of this tight junction was obviously reversed (see Fig. 4D).

RO Inhibited the Cell Viability, Migration, and Capacity of Mediating Collagen Gel Contraction in TGFβ1-Treated ARPE-19 Cells

To evaluate the effect of RO on cell function during EMT, cell viability, migration, and contractile function were examined under different conditions. The MTT assay was used to assess the cell viability and proliferation in TGFβ1-treated ARPE-19 cells with or without RO treatment. In Figure 5A, the cell viability of ARPE-19 cells was significantly increased by 38.27% ($P < 0.01$) after TGFβ1 treatment, which was partially reversed time-dependently by RO.

Transwell migration and scratch assays were carried out to measure the change of cell migration among the Vehicle, the TGFβ1 + vehicle, and the TGFβ1 + RO groups. As shown in Figure 5B, compared with the Vehicle group, the migrated RPE cells through the Transwell membrane were evidently increased in TGFβ1 treatment group, which was significantly decreased by RO treatment. Consistently, as compared with the Vehicle group, the decreased scratch area caused by TGFβ1 was also significantly inhibited by RO (Fig. 5C). Furthermore, collagen gel contraction assay demonstrated that TGFβ1-treated ARPE-19 cells exhibited a stronger ability to mediate the gel contraction when compared to untreated cells, which was significantly reduced by RO treatment (Fig. 5D). The above results further confirmed the inhibitory effect of RO on EMT in TGFβ1-treated RPE cells.

RO Suppressed the Activation of Notch Signaling Pathway in TGFβ1-Treated ARPE-19 Cells

Previous results suggested that Notch pathway activation was involved in subretinal fibrosis in laser-induced mice (see Fig. 2C). To further determine the involvement of Notch signaling in TGFβ1-treated ARPE-19 cells, we incubated the cells with TGFβ1 for 1 to 24 hours. As shown in Figure 6, TGFβ1 significantly upregulated the expressions of Notch ligand Jag1 and DLL4 (see Fig. 6A), as well as the expressions of γ-secretase components including nicastrin, presenilin 1 and 2, and PEN2 (see Fig. 6B). Expectedly, the NICD (cleaved Notch1) was significantly increased in TGFβ1 treatment group time-dependently, whereas Notch1 was significantly decreased accordingly (see Fig. 6C). The activation of Notch signaling in the TGFβ1 treatment group was further

Investigative Ophthalmology & Visual Science

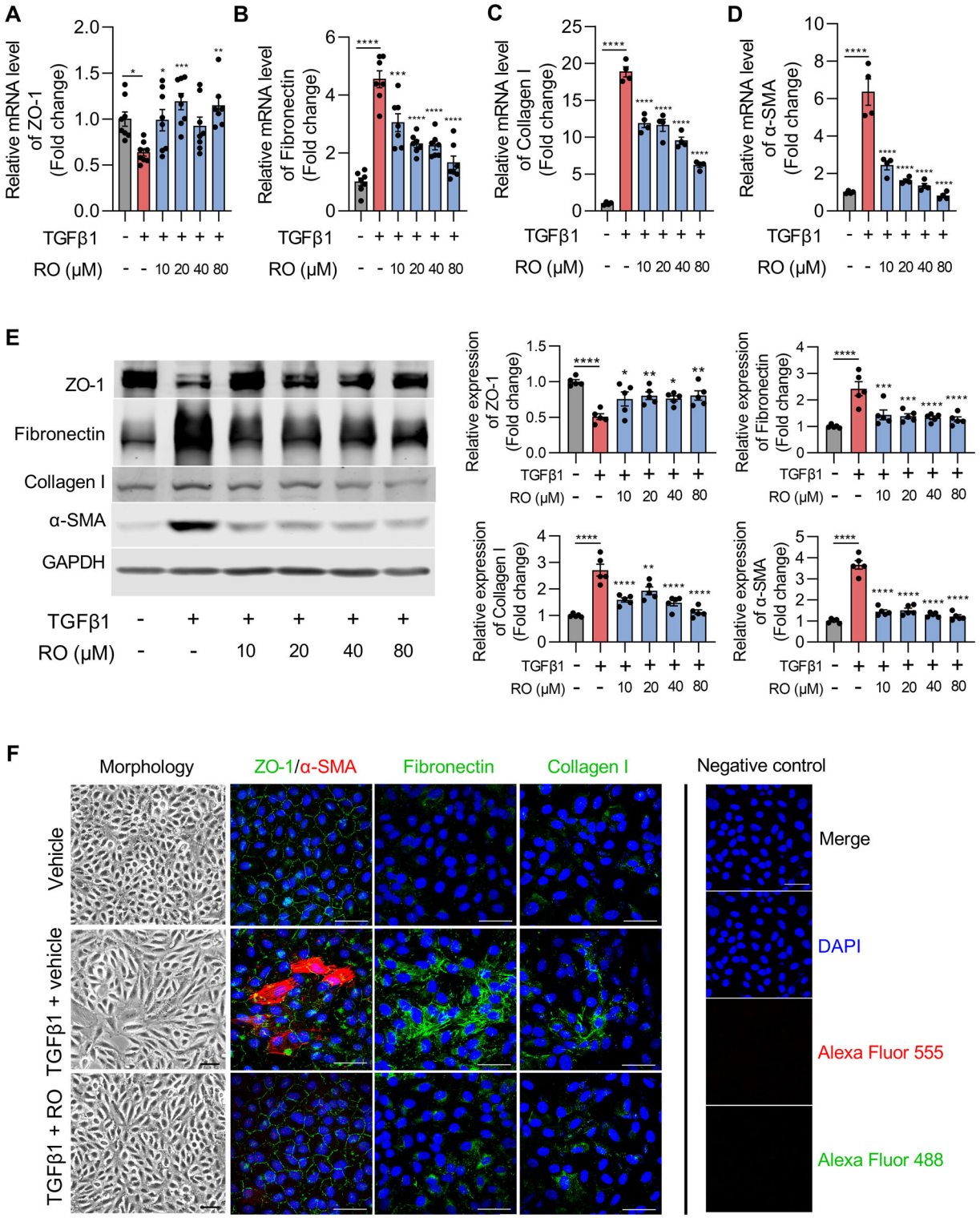

Figure 3. The effect of RO on EMT in TGFβ1-treated ARPE-19 cells. RT-qPCR for ZO-1 (**A**) and EMT-related genes, including fibronectin (**B**), collagen I (**C**), and α-SMA (**D**) in TGFβ1-treated ARPE-19 cells for 48 hours with or without different concentrations of RO treatment from 10 to 80 μM ($n = 4 - 8$ biological replicates). (**E**) Western blot analysis of ZO-1 and EMT markers among different groups ($n = 5$ biological replicates). (**F**) The change of morphology and immunostainings of the above four proteins among the Vehicle, the TGFβ1 + vehicle, and the TGFβ1 + RO (40 μM) groups. Data are expressed as mean ± SEM. * $P < 0.05$, ** $P < 0.01$, *** $P < 0.001$, **** $P < 0.0001$; 1-way ANOVA with Tukey's multiple comparisons test. Scale bar = 20 μm **F**. RO, RO4929097; Vehicle, 4 μM HCl and 0.4% DMSO; vehicle, 0.4% DMSO.

Investigative Ophthalmology & Visual Science

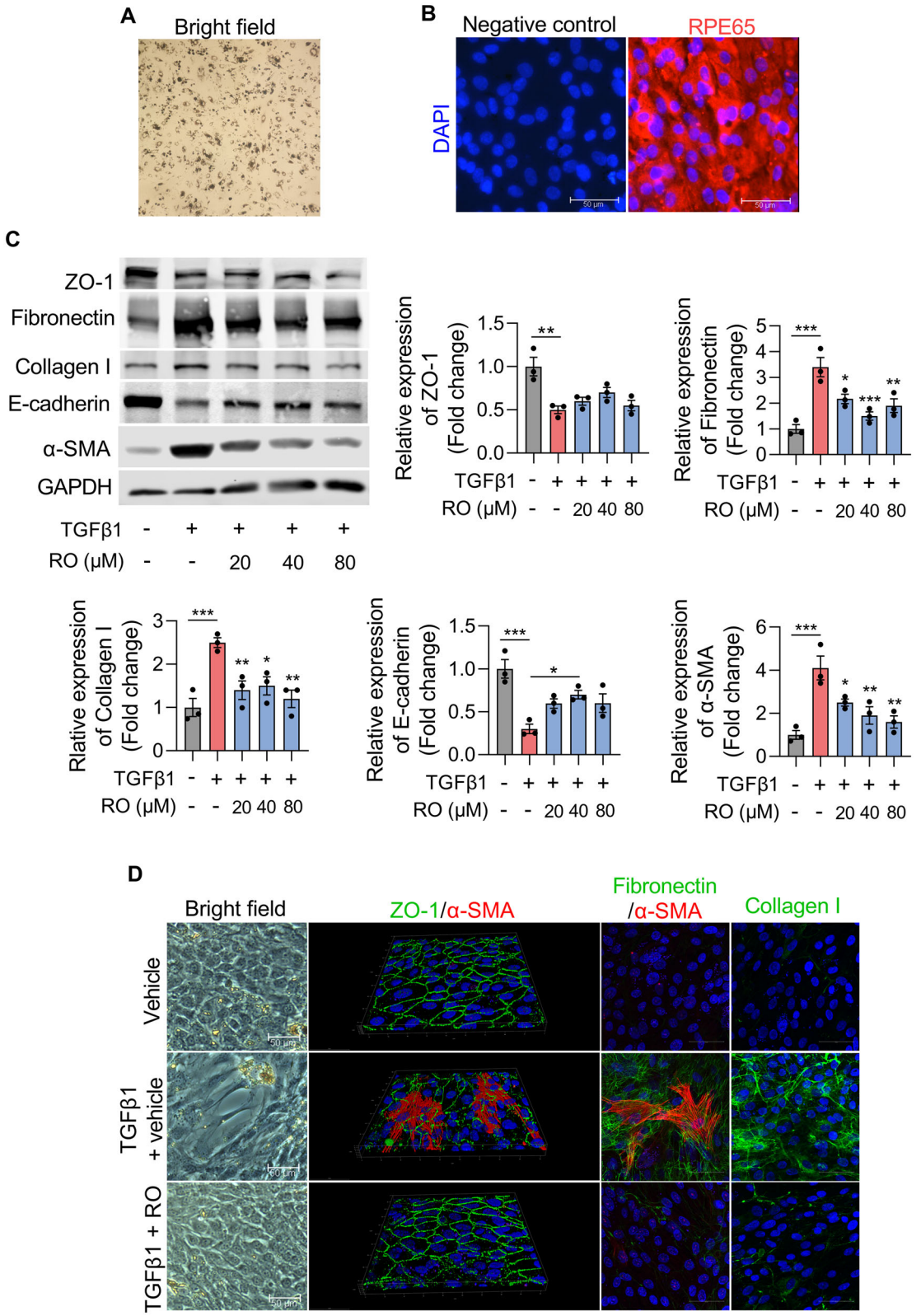

Figure 4. The effect of RO on EMT in TGFβ1-treated primary human RPE (phRPE) cells. (**A**) Bright field image of isolated phRPE cells at passage 1. (**B**) Representative image of RPE65 (a RPE cell marker) immunostaining in phRPE cells. (**C**) The change of protein levels of ZO-1, E-cadherin, ECM proteins (fibronectin and collagen I), and α-SMA in TGFβ1-treated phRPE cells for 48 hours with or without RO co-incubation at the concentrations of 20, 40, and 80 μM examined with Western blot ($n = 3$ biological replicates). (**D**) Bright field images and immunofluorescence for above proteins among the Vehicle, the TGFβ + vehicle, and the TGFβ + RO groups. Data are expressed as mean ± SEM. * $P < 0.05$, ** $P < 0.01$, *** $P < 0.001$, **** $P < 0.0001$; 1-way ANOVA with Tukey's multiple comparisons test **C**. Scale bar = 50 μm **B** and **D**. RO, RO4929097; Vehicle, 4 μM HCl and 0.4% DMSO; vehicle, 0.4% DMSO.

Investigative Ophthalmology & Visual Science

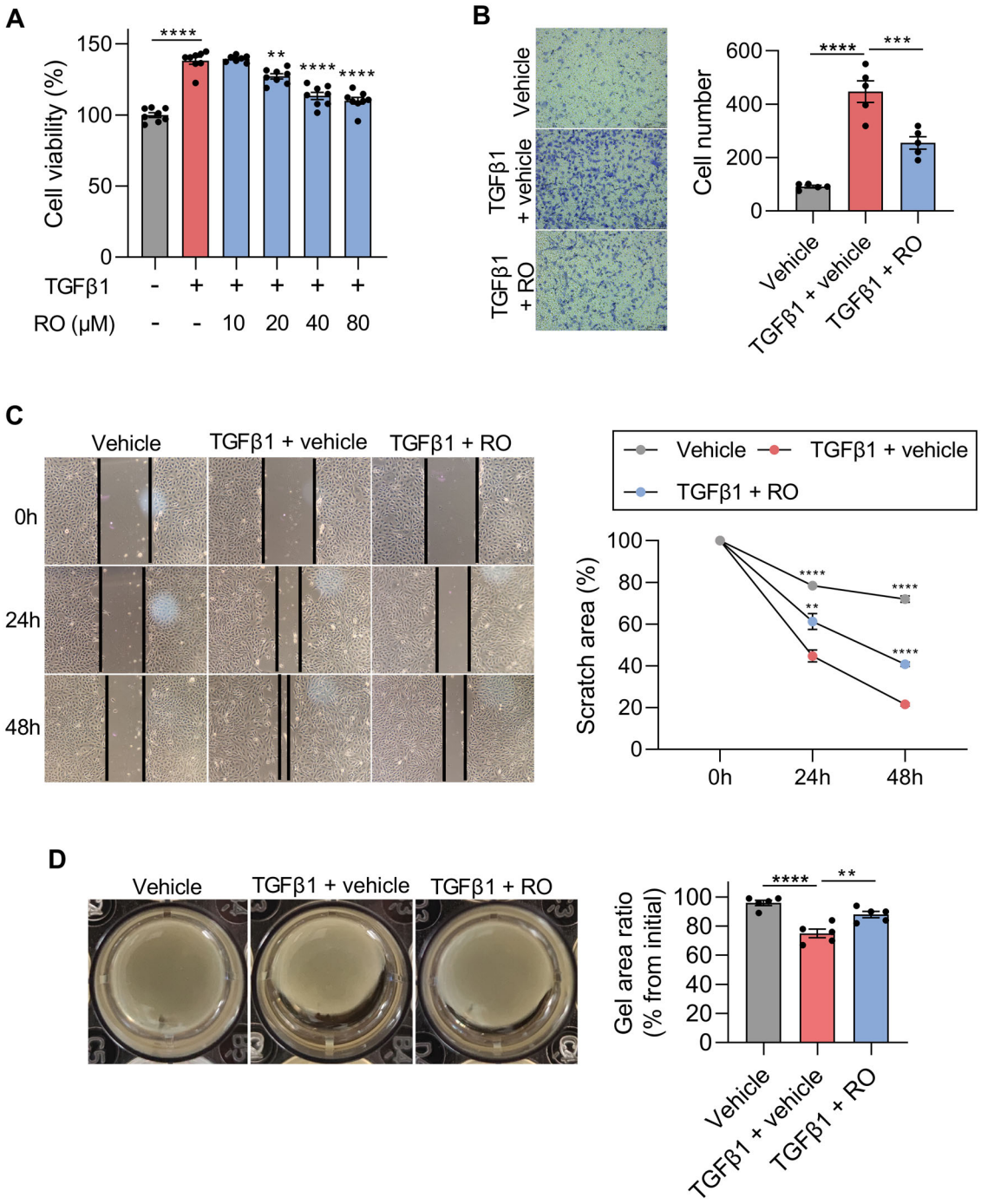

Figure 5. The effect of RO on EMT-related cell function in TGFβ1-treated ARPE-19 cells. (**A**) The change of cell viability in TGFβ1-treated ARPE-19 cells with or without different concentrations of RO co-incubation for 48 hours by using MTT assay ($n = 8$ biological replicates). (**B**) Evaluation of cell migration among the Vehicle, the TGFβ1 (10 ng/mL) + vehicle, and the TGFβ1 + RO (40 μM) groups by using Transwell migration assay ($n = 5$ biological replicates). (**C**) Scratch assay was used to confirm the change of migration among above three groups ($n = 5$ biological replicates). (**D**) Representative images of collagen gel contraction assay under different conditions ($n = 5$ biological replicates). Data are expressed as mean ± SEM. * $P < 0.05$, ** $P < 0.01$, *** $P < 0.001$, **** $P < 0.0001$; 1-way ANOVA with Tukey's multiple comparisons test. Scale bar = 250 μm **B**. RO, RO4929097; Vehicle, 4 μM HCl and 0.4% DMSO; vehicle: 0.4% DMSO.

confirmed by the upregulation of Notch downstream effector Hes1 (see Fig. 6C).

To evaluate the effect of RO on Notch activation in this EMT cell model, 40 μM of RO was used to co-incubate ARPE-19 cells for 12 hours. In Figure 6D, the activation of Notch signaling in TGFβ1-treated ARPE-19 cells, as indicated by the upregulation of Notch related molecules, including γ-secretase components, NICD and Hes1, were significantly suppressed by RO to nearly vehicle level. These data indicated that RO was able to inhibit EMT of RPE cells by effectively blocking Notch signaling pathway.

Furthermore, a side-by-side comparison in inhibition of Notch signaling and EMT was performed between RO and DAPT (one GSI) in TGFβ1-treated ARPE-19 cells. As shown

Investigative Ophthalmology & Visual Science

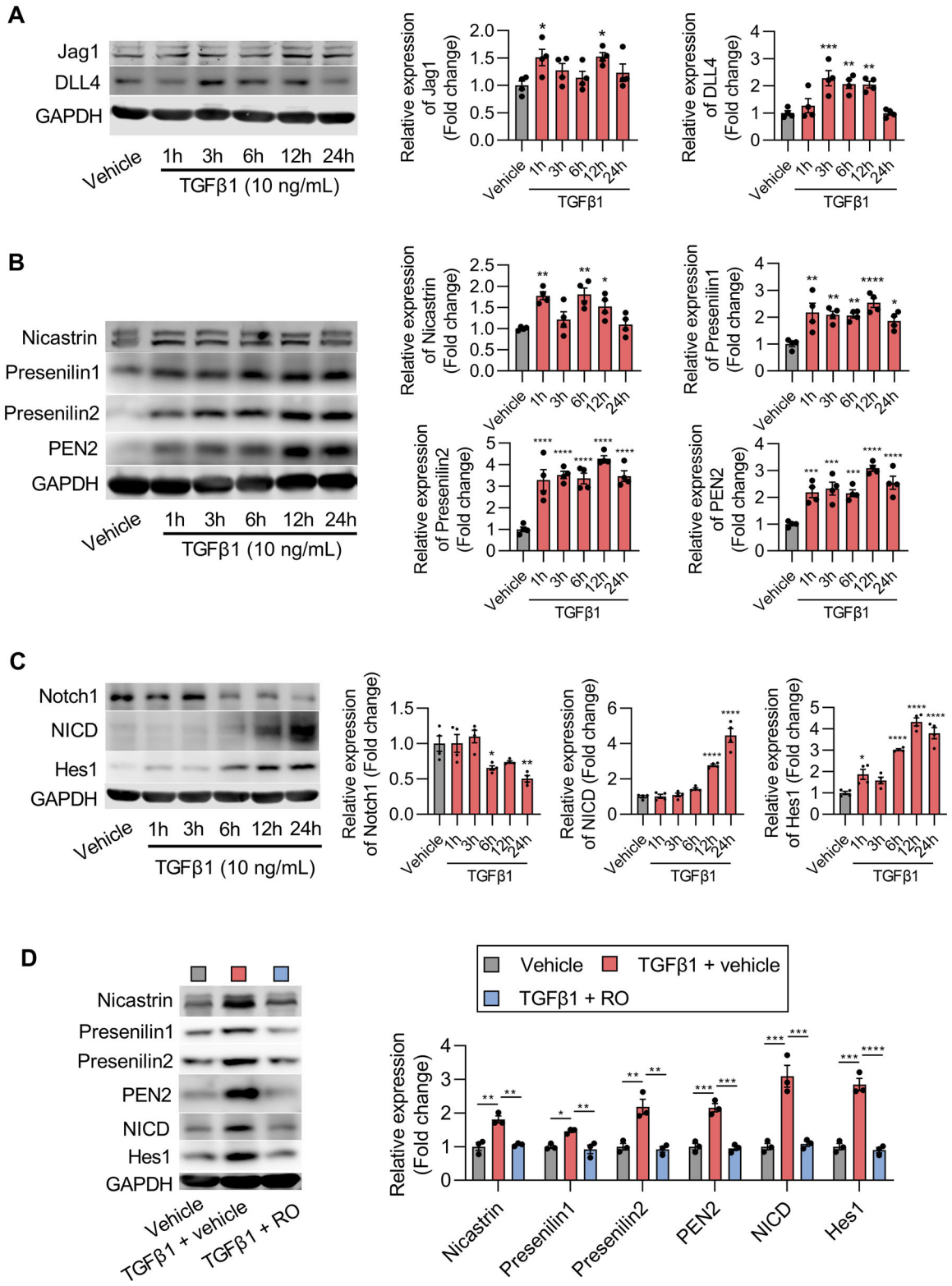

Figure 6. The change of Notch signaling pathway in TGFβ1-treated ARPE-19 cells with or without RO treatment. (**A**) Western blot analysis of Notch ligands (Jag1 and DLL4) in TGFβ1-treated ARPE-19 cells from 1 to 24 hours ($n = 4$ biological replicates). (**B**) Western blot for γ-secretase proteinases including nicastrin, presenilin 1 and 2, and PEN2 in TGFβ1-treated ARPE-19 cells ($n = 4$ biological replicates). (**C**) The change of NICD and Notch downstream effector Hes1 among different groups ($n = 4$ biological replicates). (**D**) The change of protein levels of Notch related molecules in TGFβ1-treated ARPE-19 cells with or without RO treatment (40 µM) for 12 hours ($n = 3$ biological replicates). Data are expressed as mean ± SEM. * $P < 0.05$, ** $P < 0.01$, *** $P < 0.001$, **** $P < 0.0001$; 1-way ANOVA with Tukey's multiple comparisons test. RO, RO4929097; Vehicle, 4 µM HCl **A**, **B**, and **C**, 4 µM HCl and 0.4% DMSO **D**; vehicle: 0.4% DMSO **D**.

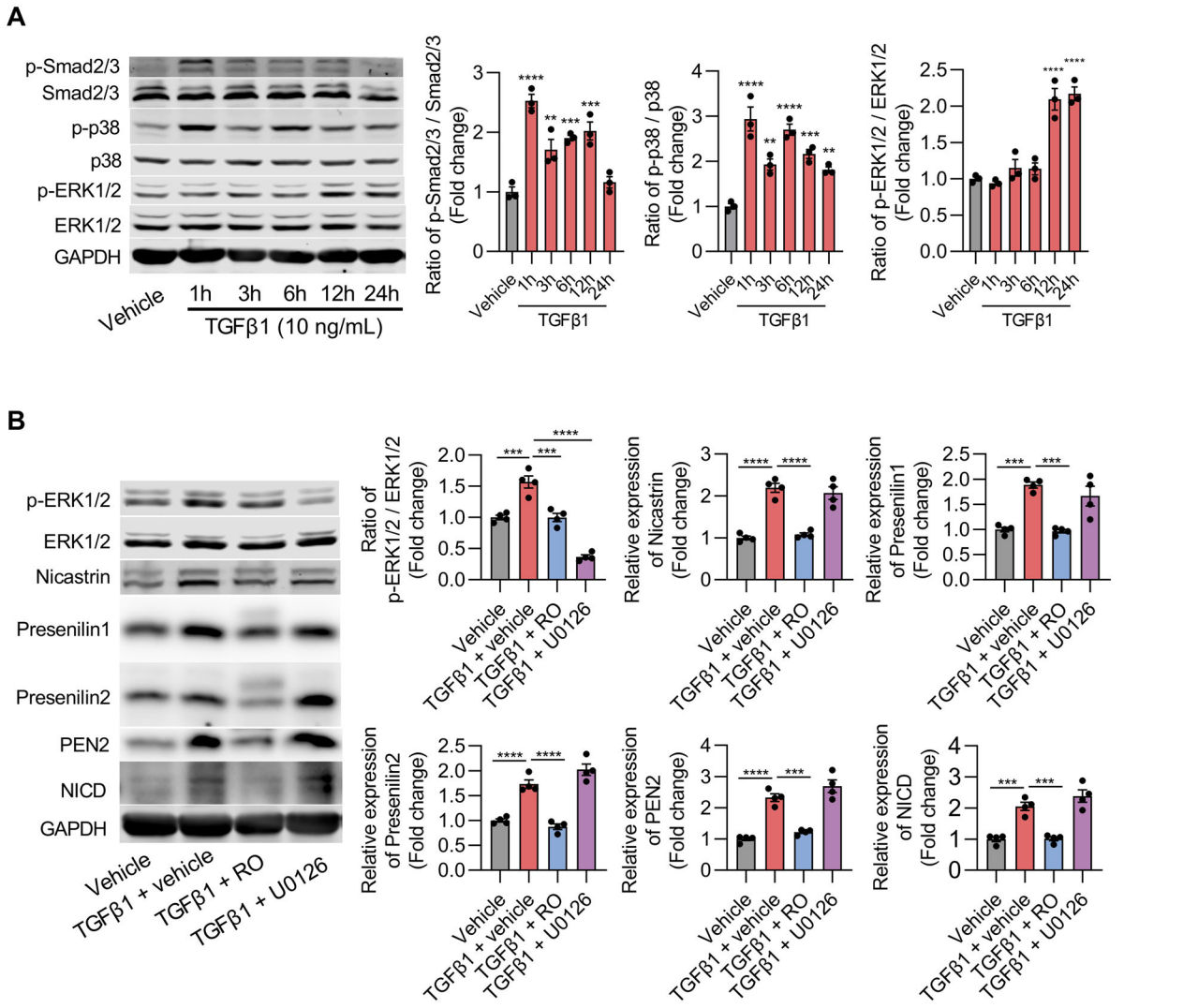

Figure 7. The interaction between Notch and other EMT-related signaling pathways. (**A**) Western blot analysis of Smad2/3, p38, and ERK1/2 in TGFβ1-treated ARPE-19 cells from 1 to 24 hours ($n = 3$ biological replicates). (**B**) The change of ERK1/2 and Notch-related molecules in TGFβ1-treated ARPE-19 cells with or without RO or U0126 treatment at 12 hours ($n = 4$ biological replicates). Data are expressed as mean ± SEM. * $P < 0.05$, ** $P < 0.01$, *** $P < 0.001$, **** $P < 0.0001$; 1-way ANOVA with Tukey's multiple comparisons test. RO, RO4929097; Vehicle, 4 µM HCl **A**, 4 µM HCl and 0.4% DMSO **B**; vehicle, 0.4% DMSO **B**.

in Supplementary Figure S5A, RO showed higher efficiency than DAPT in inhibiting Notch-related molecules presenilin1 ($P = 0.09$), NICD ($P < 0.05$), and Hes1 ($P < 0.05$). Besides, the same trend was also observed in EMT inhibition (i.e. downregulation of EMT-related markers fibronectin and α-SMA), as well as decreased cell migration mediated by RO treatment in TGFβ1-induced ARPE-19 cells was more pronounced than those by DAPT (see Supplementary Figs. S5B, S5C).

RO Suppressed ERK1/2 in TGFβ1-Treated ARPE-19 Cells

It was well documented that canonical TGFβ/Smad signaling and MAPKs were involved in the pathogenesis of EMT.[12,40] Therefore, we investigated the crosstalk between Notch with the other EMT relevant signaling pathways in ARPE-19 cells incubated with TGFβ1 for 1 to 24 hours. As shown in Figure 7A, the phosphorylation of Smad2/3, p38, and ERK1/2 was significantly increased at different time points in TGFβ1-treated ARPE-19 cells (i.e. Smad2/3 and p38 was activated from 1 hour, whereas ERK1/2 was activated at 12 and 24 hours after TGFβ1 treatment).

To explore the effect of RO on ERK1/2 signaling, 40 µM of RO was used in TGFβ1-treated ARPE-19 cells for 12 hours. In Figure 7B, the activation of ERK1/2 at 12 hours after TGFβ1 treatment was significantly inhibited by RO treatment, whereas the ERK1/2 specific inhibitor U0126 showed no effect on γ-secretase proteinases and NICD in TGFβ1-treated ARPE-19 cells. These data indicated Notch and γ-secretase might be the upstream molecules of ERK1/2 signaling.

To further investigate the relationship of Notch with the other EMT relevant signaling pathways, SB431542 (SB, inhibitor of ALK5 which phosphorylates Smad2/3) and Adezmapimod (Ad, inhibitor of p38 MAPK) were used. As shown in Figure 8A, RO showed no obvious effect on the activation of Smad2/3 and p38 in ARPE-19 cells induced by TGFβ1 for 1 hour. Moreover, in Figure 8B, TGFβ1 induced

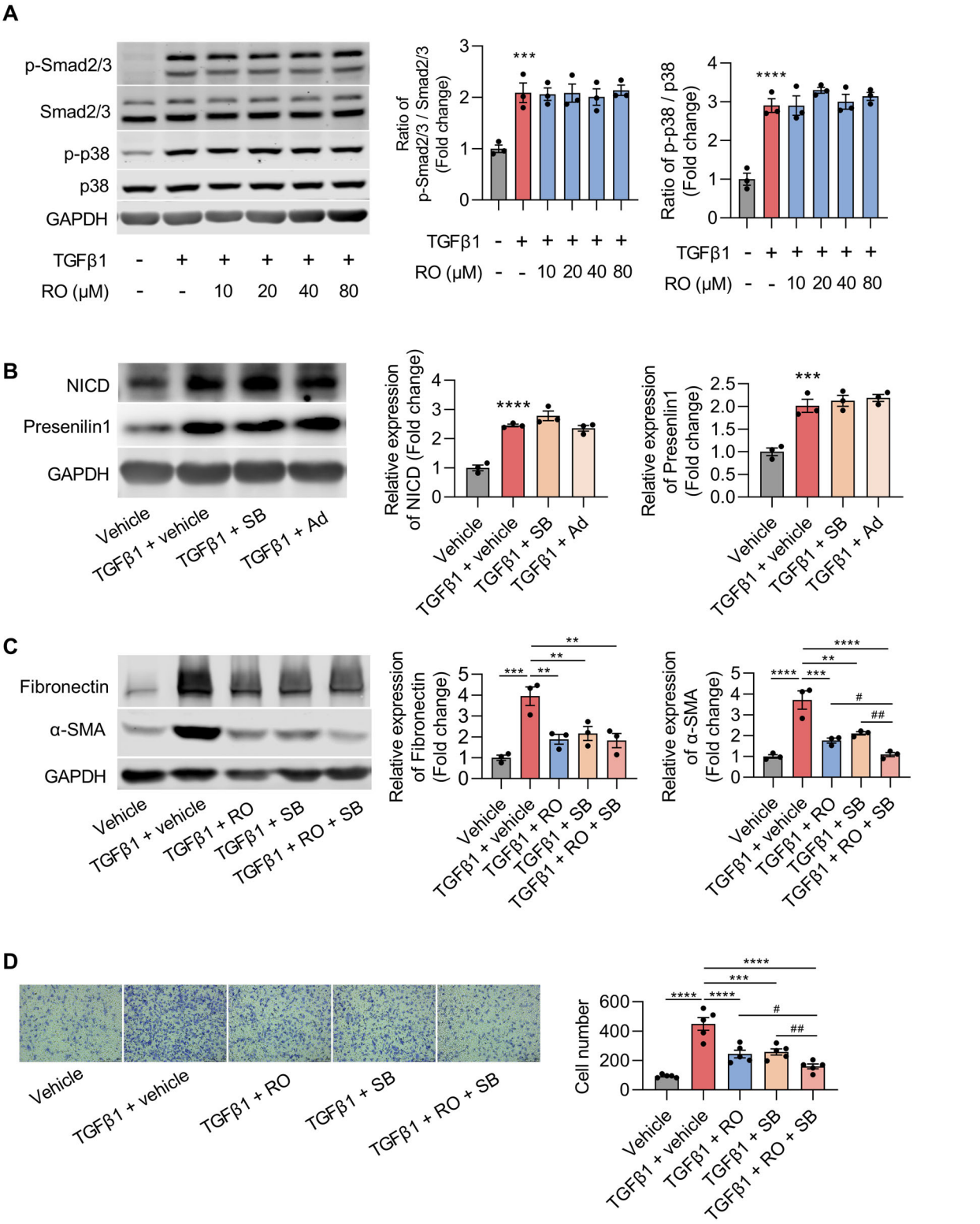

Figure 8. The additive effect of inhibition of both Notch signaling and Smad2/3 on EMT in TGFβ1-induced ARPE-19 cells. (**A**) Western blot analysis of p-Smad2/3 and p-p38 in TGFβ1-treated ARPE-19 cells with or without RO (10 to 80 μM) treatment ($n = 3$ biological replicates). (**B**) The changes of NICD and presenilin1 expression in TGFβ1-treated ARPE-19 cells for 12 hours with or without pre-treatment of SB (10 μM) or Ad (10 μM) for 1 hour ($n = 3$ biological replicates). (**C**) The protein levels of fibronectin and α-SMA in TGFβ1-treated ARPE-19 cells with or without treatment of RO, SB, or a combination of both for 48 hours ($n = 3$ biological replicates). (**D**) The change of ARPE-19 cell migration among above five groups by using Transwell assay ($n = 5$ biological replicates). Data are expressed as mean ± SEM. * $P < 0.05$, ** $P < 0.01$, *** $P < 0.001$, **** $P < 0.0001$; # $P < 0.05$, ## $P < 0.01$; 1-way ANOVA with Tukey's multiple comparisons test. RO, RO4929097; Vehicle, 4 μM HCl and 0.1 to 0.4% DMSO; vehicle, 0.1 to 0.4% DMSO. SB, SB431542; Ad, Adezmapimod.

upregulation of NICD and presenilin1 remained unchanged with addition of SB or Ad. These data suggested that the relationship between Notch and Smad2/3 or p38 might be independent.

Co-Inhibition of Notch and Smad2/3 Showed Synergistic Effect on the TGFβ1-Induced EMT in ARPE-19 Cells

We next examined whether Notch and Smad2/3 inhibitors had additive effect on suppressing EMT in TGFβ1-treated ARPE-19 cells. ARPE-19 cells in the TGFβ1 + vehicle group were incubated with or without RO, SB, or a combination of both for 48 hours. As shown in Figure 8C, the upregulation of EMT marker α-SMA in the TGFβ1 + vehicle group was reversed by RO, SB, or RO + SB, with the most significant and additive effect in the RO + SB group. In addition, the upregulation of ECM protein fibronectin in TGFβ1-treated ARPE-19 cells was also inhibited by RO, SB, or RO + SB, but without additive effect in the RO + SB group. The cell migration among above five groups was also studied and the result showed that the combination of RO + SB exerted a synergistic effect in inhibiting cell migration in TGFβ1-treated ARPE-19 cells (Fig. 8D).

Discussion

CNV and subretinal fibrosis are two major pathological features of nAMD, which lead to structural and functional damage of RPE cells and photoreceptors, and subsequent irreversible central vision loss.[16] The EMT exerts a physiological role in wound healing and embryonic development, but its dysfunction could result in severe adverse effects, such as carcinogenesis and fibrosis.[16,40] Increasing evidence suggested EMT driven by TGFβ/Smad signaling contributes significantly to the formation and development of subretinal fibrosis in both patients with nAMD and experimental animal models.[11,15,41] Importantly, it was reported that the Notch activation contributed to the pathogenesis of PVR through promoting EMT, which could be prevented by a gamma-secretase inhibitor (GSI) LY411575.[28] These above reports indicated that Notch signaling was also involved in the EMT and subretinal fibrosis formation, and therefore blockage of Notch signaling might provide a promising strategy to prevent and treat subretinal fibrosis. However, whether or not Notch signaling contributes to subretinal fibrosis secondary to laser-induced CNV still remained largely unknown.

In this study, by using laser-induced CNV mice, we explored the involvement of Notch signaling in subretinal fibrosis and EMT, as well as the possible inhibitory effect of RO (a specific GSI). The preliminary data showed that intravitreal injection of RO suppressed CNV and subretinal fibrosis in both young and old laser-induced CNV mice (see Fig. 1) via inhibiting γ-secretase and Notch signaling (see Fig. 2C), further confirming the contribution of Notch signaling in subretinal fibrosis in laser-induced CNV mice. Moreover, colocalization of RPE65 and α-SMA in CNV lesion suggested the involvement of EMT in the formation of subretinal fibrosis, and RO also obviously inhibited the RPE-derived myofibroblast (RPE65 + and α-SMA +) through EMT (see Fig. 2B). These data suggested that the inhibitory effect of RO on subretinal fibrosis might be due to its anti-EMT role in laser-induced CNV mice.

The cellular and molecular components of CNV lesion and subretinal fibrosis are important issues in this field. Histological studies of human tissue and preclinical studies revealed that choroidal neovascular membranes are composed of different cell types including RPE cells, vascular endothelial cells, glial cells, microglia, macrophages, pericytes, fibroblast-like cells, and myofibroblasts.[7] Myofibroblasts, typically expressing α-SMA and depositing pathological ECM, are the key element of subretinal fibrosis. Because myofibroblasts are absent in the healthy macula, they are supposed to be transdifferentiated from multiple myofibroblast precursor cells, such as RPE cells, macrophages, Müller cells, vascular endothelial cells, and pericytes, as well as circulating fibrocytes.[42] Among the potential candidates of the origin of myofibroblasts, RPE cells undergoing EMT are considered a major source of myofibroblasts.[11,43] To compare the proportions of pericytes and RPE cells in our laser-induced CNV mice, ImageJ software with the Coloc 2 plugin was used to analyze the colocalization of the α-SMA immunostaining with PDGFRβ and RPE65, respectively. Pearson's correlation coefficient (PCC) is the most commonly used correlation coefficient to quantitatively describe colocalization, and its value ranges from 1 to -1. Manders' Colocalization Coefficients (MCC) represents the proportion of the colocalized region to the total content of one protein immunoreactivity. The statistical analysis data showed that, PCC of α-SMA and PDGFRβ, and α-SMA and RPE65 was 0.35 and 0.38, respectively, indicating the similar level of colocalization with α-SMA between pericytes and RPE cells. In addition, after normalization by α-SMA immunoreactivity, MCC of α-SMA and PDGFRβ, and α-SMA and RPE65 was 0.349 vs. 0.436, suggesting a larger proportion of transdifferentiated RPE cells (43.6%) than pericytes (34.9%) in the α-SMA + CNV lesion. Considering the limitation of the nonspecific labeling of α-SMA for pericytes and myofibroblasts, the involvement of EMT in subretinal fibrosis might be much more than pericyte-myofibroblast transition (PMT). It was reported that approximately 20% of infiltrating Iba-1 + myeloid cells in human macular fibrosis were reported to be immunoreactive for α-SMA,[44] suggesting that macrophage to myofibroblast transition (MMT) is also present in macular fibrosis secondary to nAMD. Overall, transdifferentiated RPE cells undergoing EMT might be the primary cellular component in subretinal fibrosis in laser-induced CNV mice.

To confirm the anti-EMT effect of RO, TGFβ1-inducd EMT cell model was used to test the inhibitory effect of RO on EMT. The results showed that Notch ligands, γ-secretase components, NICD, and Notch downstream effector Hes1 were evidently upregulated after TGFβ1 treatment (see Fig. 6), leading to the upregulation of ECM proteins and decreased tight junction protein (see Figs. 3, 4), as well as enhanced cell viability, migration, and contractile function (see Fig. 5). The above changes were significantly reduced by RO. Collectively, our findings indicated that the activation of Notch signaling contributed to subretinal fibrosis via EMT, whereas inhibition of Notch signaling could be a new strategy to prevent subretinal fibrosis through inhibiting EMT.

Compared to other GSIs, DAPT and LY411575, two well studied GSIs in subretinal fibrosis and EMT,[45] RO displayed superiorities in its high efficiency and clinical translation. Among GSIs, DAPT, LY411575, and RO belong to the peptidomimetics-based GSIs, binding to an allosteric site in the γ-secretase complex and affecting its activity, which form the largest and most diverse set of GSIs.[46,47] Increasing evidence suggested that GSIs displayed distinguishing

Investigative Ophthalmology & Visual Science

efficiencies in inhibiting Notch cleavage by using cell-based γ-secretase cleavage assay. One recent study showed that half maximal inhibitory concentration (IC_{50}) of DAPT and RO on recombinant human Notch1 substrate were 4.90 nM and 0.46 nM, respectively.[32] Whereas LY411575 inhibited Notch cleavage with IC_{50} of 0.39 nM in amyloid precursor protein or truncated Notch1 expressing HEK293 cells.[48] Another report using a dual substrate assay (an improved cell-based method) found that LY411575 also demonstrated much higher efficacy than DAPT in suppression of NICD production, as indicated by the values of NICD IC_{50} 1.3 nM vs. 360 nM.[49] These data indicated that, in terms of inhibition efficiency, both LY411575 and RO were comparable and stronger than DAPT. Furthermore, RO is a close analog of LY411575 from a classic example of the allosteric inhibitor series compound E. The displacement of the 3,5-difluorobenzyl group with a pentafluoropropyl group has improved the metabolic stability of the compound (RO4929097), making it suitable for clinical and biological studies.[46] Actually, LY411575 related research is just at the preclinical status without any clinical trials (data from *ClinicalTrials.gov*). To further verify the superiority of RO, a side-by-side comparison was performed between RO and DAPT in the inhibition of Notch signaling and EMT in TGFβ1-treated ARPE-19 cells (see Supplementary Fig. S5), which confirmed the superior efficiency of RO than DAPT.

Controversy still exists regarding the role of the TGFβ in nAMD. One study revealed that TGFβ1 in the aqueous humor of patients with naïve CNV was significantly higher compared with controls in a VEGFA-independent manner[50]; whereas the other clinical research showed an anti-angiogenic role of TGFβ2 in nAMD.[51] In addition, TGFβ signaling is constitutively active in normal retina (e.g. TGFβ exerts pleiotropic effects on multiple retinal cell types that underlie numerous functions), including maintaining retinal neuronal differentiation and survival,[52,53] regulating the development and structural integrity of retinal vessels,[54] as well as the normal organization of microglia in the healthy retina.[55] For example, TGFBR2-deficient microglia demonstrated exaggerated responses to laser-induced injury, as indicated by increased CNV.[55] Therefore, a general inhibition of TGFβ, such as using its antibody, should be viewed with caution, and the strategies targeting the specific isoform of TGF-β and targeting specific cell population are suggestive, which merit further exploration.

There is increasing evidence that TGFβ and Notch signaling pathways synergistically result in fibrosis formation.[56–58] It was reported that incubation of Müller cells with TGFβ or Notch ligands activated each signaling pathway profoundly.[33] In our study, we found TGFβ1 could also significantly activate the Notch signaling in ARPE-19 cells. Therefore, we next focused on the crosstalk among Notch, the canonical TGFβ/Smad2/3 signaling, and other noncanonical signaling, such as MAPKs,[59] which were also activated in TGFβ1-treated ARPE-19 cells (see Fig. 7A). Our data demonstrated that inhibition of Notch signaling by RO could significantly suppress the activation of ERK1/2 in TGFβ1-treated ARPE-19 cells at 12 hours, whereas blockage ERK1/2 showed no effect on Notch signaling (see Fig. 7B), indicating that Notch might be the upstream signaling of ERK1/2. One study showed that, in TGFβ2-treated ARPE-19 cells at 0.5 hours, treatment of ARPE-19 cells with ERK1/2 or Notch inhibitor suppressed each other's signaling.[29] This discrepancy between these two studies might be attributed to the different TGFβ isoforms used, as well as the different time point. However, in our study, TGFβ1 treatment showed no effect on the phosphorylation of ERK1/2 at 0.5 hours (Supplementary Fig. S6B), but activated this signaling at 12 and 24 hours (see Fig. 7A). Several other studies also reported that GSI suppressed ERK1/2 signaling in cancer research,[60,61] but few clarified the specific mechanism. It was reported that GSI treatment inhibited ERK1/2 through upregulating DUSP1, a possible mediator in the cross-talk between Notch and ERK1/2, because Notch downstream effector Hes1 directly binds to and represses the promoter of *DUSP1*, encoding a dual phosphatase that is active against phospho-ERK.[62] In addition to ERK1/2, our results suggested that RO showed no effect on the TGFβ1-induced activation of Smad2/3 and p38 in ARPE-19 cells (see Fig. 8A), and Smad2/3 or p38 inhibitor did not affected the Notch signaling, suggesting the independent relationship between Notch and Smad2/3 or p38 (see Fig. 8B). Considering the critical role of canonical TGFβ/Smad2/3 and its independent relationship with Notch, we hypothesized that the combined inhibition of these two pathways might have an additive therapeutic effect on EMT inhibition. The result showed that combination of Notch and Smad2/3 inhibitors showed a additive inhibition on EMT than single treatment (see Figs. 8C, 8D), thus providing a new therapeutic option for subretinal fibrosis.

It should be noted that RO not only inhibited subretinal fibrosis, but also suppressed the CNV in laser-induced mice (see Fig. 1). In angiogenesis, it has been widely accepted that Notch directs proliferation and specification of endothelial cell,[63] but its role in CNV is complicated because it might play different roles in different cell types.[64,65] Several studies reported that activation of Notch signaling could inhibited CNV in laser-induced CNV mice.[30,31,65] However, two studies reported the different effect of intraocular injection of GSI DAPT on CNV with different dosage used. In the first study, laser-induced CNV lesion volume remained unchanged after intravitreal injection of DAPT (16 ng/eye; 37 µM for 1 µL) in laser-induced CNV mouse model, even though the angiogenesis was inhibited by γ-secretase upregulation via either pigment epithelium derived factor or presenilin1 overexpression.[30] Whereas the second study showed a higher concentration of DAPT (200 µg/eye; 462.47 mM for 1 µL) exacerbated laser-induced CNV lesions in a rat model.[31] The dosage of RO used in our study was 100 µM for 1 µL, which was able to evidently attenuate both CNV and subretinal fibrosis, as well as Notch signaling activation, in laser-induced CNV mice (see Figs. 1, 2C). The discrepancy of CNV change among these three studies might be due to the different dosage of GSIs. Mild inhibition of Notch pathway showed no obvious effect on CNV (the first study), whereas strong inhibition of Notch pathway aggravated CNV in laser-induced rat model (the second study). Considering the differences of efficiency in γ-secretase inhibition between RO and DAPT as well as the different volume of vitreous cavity between the rat and mouse, the Notch inhibition by RO (100 µM for 1 µL/eye) used in our study was 30 times stronger than that of DAPT (16 ng/eye; 37 µM for 1 µL) used in the first study, but much lower than DAPT (200 µg/eye; 462.47 mM for 1 µL) used in the second study (about 1/100). Besides, we speculated that the CNV inhibition by RO might be due to its secondary effect of antifibrotic action in laser-induced CNV mice. In laser-induced mouse model, CNV and fibrosis interdependent. Subretinal fibrosis in nAMD develops from existing neovascular membrane. If the neovascular membrane is inhibited and regressed at the very early stage

Investigative Ophthalmology & Visual Science

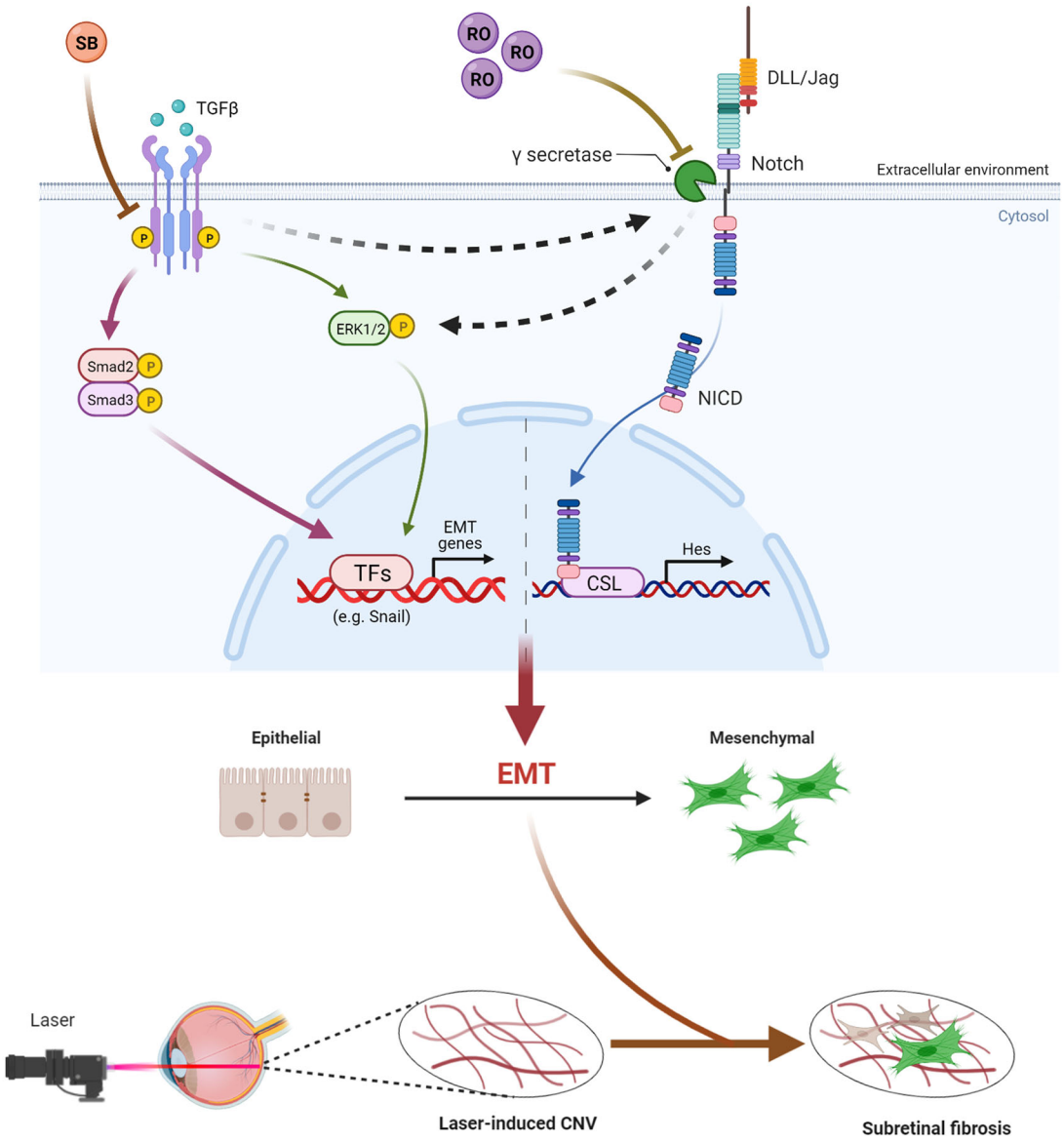

Figure 9. Schematic diagram depicting the mechanisms of RO in inhibiting subretinal fibrosis secondary to laser-induced CNV. In TGFβ-treated RPE cells, the activation of Notch signaling resulted in EMT, which contributed to the pathogenesis of subretinal fibrosis in laser-induced CNV. RO, a specific γ secretase inhibitor, exerts its protective effect by directly suppressing Notch activation and indirectly inhibiting ERK1/2 to prevent subretinal fibrosis and EMT in laser-induced CNV mice. Moreover, combination of Notch and Smad2/3 inhibitors showed an additive role in blocking EMT. RO, RO4929097; SB, SB431542 (Smad2/3 inhibitor).

of nAMD, fibrosis is unlikely to occur.[7] Conversely, recruitment and activation of myofibroblasts as the perivascular mural cells during the disease progression might contribute to neovascular remodeling complicating nAMD.[66] Therefore, our work demonstrated that RO, at a moderate and optimal concentration, significantly suppressed subretinal fibrosis and subsequent neovascular remodeling in laser-induced CNV mice.

There are several limitations of this study. In this study, we found both the sizes of CNV and subretinal fibrosis were reduced in laser-induced CNV mice by RO intravitreal injection. We just speculated that the CNV inhibition by RO might be due to its secondary effect of antifibrotic action in laser-induced CNV mice, but did not explore the specific mechanism of RO in CNV reduction (see Fig. 1, Supplementary Fig. S2), which merits further study. In addition, the combined therapy with Notch and Smad2/3 inhibitors in laser-induced CNV mouse model deserves further investigation. It is also meaningful to elucidate the specific mechanism or mediator involved in the indirect inhibition of RO on ERK1/2.

In summary, as indicated by the schematic diagram in Figure 9, our studies indicate that Notch signaling pathway contributes to subretinal fibrosis secondary to laser-induced CNV through EMT, which could be inhibited by a selective γ-secretase inhibitor RO4929097 both in vivo and in vitro. Mechanistically, RO exerts its protective effect by directly suppressing Notch activation and indirectly inhibiting ERK1/2 to prevent subretinal fibrosis and EMT in laser-induced CNV mice. Notch and Smad2/3 (or p38) are mutually independent pathways, and combination of Notch and Smad2/3 inhibitors showed synergistic effect on inhibit-

Investigative Ophthalmology & Visual Science

ing EMT. This study highlighted that inhibition of Notch signaling or combined with Smad 2/3 inhibition might provide a therapeutic strategy in prevention and treatment of subretinal fibrosis in nAMD and other fibrovascular diseases.

Acknowledgments

The authors acknowledge the support from the Laboratory of Clinical and Visual Sciences (LCVS), Tongji Eye Institute, Tongji University School of Medicine, Shanghai, China. We are also grateful to all our colleagues who were involved in this study.

Supported by the National Natural Science Foundation of China (82171062 and, 81970810) and Domestic Science and Technology Cooperation Project of Shanghai Municipal Science and Technology Commission (21015800700).

Ethics Approval: All animal experiments were approved by the Animal Research Committee at Shanghai Jiao Tong University (Permit number: 2019AW055) and conducted with strict adherence to the Association for Research in Vision and Ophthalmology (ARVO) Statement for the Use of Animals in Ophthalmic and Vision Research.

Author's Contributions: C.Y.Z. and J.F.Z. contributed to the conception and design of the experiments and were responsible for data collection, analysis, and interpretation. C.Y.Z. contributed methodology, investigation, and data curation. C.Y.Z. and J.F.Z. drafted the article and revised the article critically for important intellectual content. S.Y.Q., H.X., Q.H.Q., H.Y.W., J.T.Z., D.W.L., and J.F.Z. contributed to the data analysis and discussion. Q.H.Q., D.W.L., and J.F.Z. contributed funding support. All authors approved the final version of the manuscript for submission. J.F.Z. is the guarantor of this work, who has full access to all the data in this study and takes responsibility for the integrity and accuracy of the data.

Availability of data and materials: All data generated or analyzed during this study are included in this published article and its supplementary information files.

Disclosure: **C. Zhang**, None; **S. Qin**, None; **H. Xie**, None; **Q. Qiu**, None; **H. Wang**, None; **J. Zhang**, None; **D. Luo**, None; **J. Zhang**, None

References

1. Wong WL, Su X, Li X, et al. Global prevalence of age-related macular degeneration and disease burden projection for 2020 and 2040: a systematic review and meta-analysis. *Lancet Glob Health*. 2014;2:e106–e116.
2. Ding X, Patel M, Chan CC. Molecular pathology of age-related macular degeneration. *Prog Retin Eye Res*. 2009;28:1–18.
3. Rosenfeld PJ, Brown DM, Heier JS, et al. Ranibizumab for neovascular age-related macular degeneration. *N Engl J Med*. 2006;355:1419–1431.
4. Brown DM, Michels M, Kaiser PK, et al. Ranibizumab versus verteporfin photodynamic therapy for neovascular age-related macular degeneration: Two-year results of the ANCHOR study. *Ophthalmology*. 2009;116:57–65.e55.
5. Wu J, Zhang C, Yang Q, et al. Imaging Hyperreflective Foci as an Inflammatory Biomarker after Anti-VEGF Treatment in Neovascular Age-Related Macular Degeneration Patients with Optical Coherence Tomography Angiography. *Biomed Res Int*. 2021;2021:6648191.
6. Daniel E, Toth CA, Grunwald JE, et al. Risk of scar in the comparison of age-related macular degeneration treatments trials. *Ophthalmology*. 2014;121:656–666.
7. Little K, Ma JH, Yang N, Chen M, Xu H. Myofibroblasts in macular fibrosis secondary to neovascular age-related macular degeneration - the potential sources and molecular cues for their recruitment and activation. *EBioMedicine*. 2018;38:283–291.
8. Little K, Llorian-Salvador M, Tang M, et al. A Two-Stage Laser-Induced Mouse Model of Subretinal Fibrosis Secondary to Choroidal Neovascularization. *Transl Vis Sci Technol*. 2020;9:3.
9. Lopez PF, Sippy BD, Lambert HM, Thach AB, Hinton DR. Transdifferentiated retinal pigment epithelial cells are immunoreactive for vascular endothelial growth factor in surgically excised age-related macular degeneration-related choroidal neovascular membranes. *Invest Ophthalmol Vis Sci*. 1996;37:855–868.
10. Li M, Dolz-Marco R, Messinger JD, et al. Clinicopathologic Correlation of Anti-Vascular Endothelial Growth Factor-Treated Type 3 Neovascularization in Age-Related Macular Degeneration. *Ophthalmology*. 2018;125:276–287.
11. Ishikawa K, Kannan R, Hinton DR. Molecular mechanisms of subretinal fibrosis in age-related macular degeneration. *Exp Eye Res*. 2016;142:19–25.
12. George SM, Lu F, Rao M, Leach LL, Gross JM. The retinal pigment epithelium: Development, injury responses, and regenerative potential in mammalian and non-mammalian systems. *Prog Retin Eye Res*. 2021;85:100969.
13. Kuiper EJ, Witmer AN, Klaassen I, Oliver N, Goldschmeding R, Schlingemann RO. Differential expression of connective tissue growth factor in microglia and pericytes in the human diabetic retina. *Br J Ophthalmol*. 2004;88:1082–1087.
14. Kuiper EJ, Van Nieuwenhoven FA, de Smet MD, et al. The angio-fibrotic switch of VEGF and CTGF in proliferative diabetic retinopathy. *PLoS One*. 2008;3:e2675.
15. Hirasawa M, Noda K, Noda S, et al. Transcriptional factors associated with epithelial-mesenchymal transition in choroidal neovascularization. *Mol Vis*. 2011;17:1222–1230.
16. Wu D, Kanda A, Liu Y, Kase S, Noda K, Ishida S. Galectin-1 promotes choroidal neovascularization and subretinal fibrosis mediated via epithelial-mesenchymal transition. *FASEB J*. 2019;33:2498–2513.
17. Lai K, Li Y, Li L, et al. Intravitreal injection of triptolide attenuates subretinal fibrosis in laser-induced murine model. *Phytomedicine*. 2021;93:153747.
18. Peng X, Xiao H, Tang M, et al. Mechanism of fibrosis inhibition in laser induced choroidal neovascularization by doxycycline. *Exp Eye Res*. 2018;176:88–97.
19. Xie L, Wang Y, Li Q, et al. The HIF-1alpha/p53/miRNA-34a/Klotho axis in retinal pigment epithelial cells promotes subretinal fibrosis and exacerbates choroidal neovascularization. *J Cell Mol Med*. 2021;25:1700–1711.
20. Wilson A, Radtke F. Multiple functions of Notch signaling in self-renewing organs and cancer. *FEBS Lett*. 2006;580:2860–2868.
21. Wang Y, Shen RW, Han B, et al. Notch signaling mediated by TGF-beta/Smad pathway in concanavalin A-induced liver fibrosis in rats. *World J Gastroenterol*. 2017;23:2330–2336.
22. Romeo S. Notch and Nonalcoholic Fatty Liver and Fibrosis. *N Engl J Med*. 2019;380:681–683.
23. Liu M, Ning X, Li R, et al. Signalling pathways involved in hypoxia-induced renal fibrosis. *J Cell Mol Med*. 2017;21:1248–1259.
24. Kovall RA, Blacklow SC. Mechanistic insights into Notch receptor signaling from structural and biochemical studies. *Curr Top Dev Biol*. 2010;92:31–71.

25. Bray SJ. Notch signalling: a simple pathway becomes complex. *Nat Rev Mol Cell Biol*. 2006;7:678–689.
26. Escamilla-Ayala A, Wouters R, Sannerud R, Annaert W. Contribution of the Presenilins in the cell biology, structure and function of gamma-secretase. *Semin Cell Dev Biol*. 2020;105:12–26.
27. Luistro L, He W, Smith M, et al. Preclinical profile of a potent gamma-secretase inhibitor targeting notch signaling with in vivo efficacy and pharmacodynamic properties. *Cancer Res*. 2009;69:7672–7680.
28. Zhang J, Yuan G, Dong M, et al. Notch signaling modulates proliferative vitreoretinopathy via regulating retinal pigment epithelial-to-mesenchymal transition. *Histochem Cell Biol*. 2017;147:367–375.
29. Chen X, Xiao W, Wang W, Luo L, Ye S, Liu Y. The complex interplay between ERK1/2, TGFbeta/Smad, and Jagged/Notch signaling pathways in the regulation of epithelial-mesenchymal transition in retinal pigment epithelium cells. *PLoS One*. 2014;9:e96365.
30. Qi X, Cai J, Ruan Q, et al. gamma-Secretase inhibition of murine choroidal neovascularization is associated with reduction of superoxide and proinflammatory cytokines. *Invest Ophthalmol Vis Sci*. 2012;53:574–585.
31. Ahmad I, Balasubramanian S, Del Debbio CB, et al. Regulation of ocular angiogenesis by Notch signaling: implications in neovascular age-related macular degeneration. *Invest Ophthalmol Vis Sci*. 2011;52:2868–2878.
32. Ran Y, Hossain F, Pannuti A, et al. gamma-Secretase inhibitors in cancer clinical trials are pharmacologically and functionally distinct. *EMBO Mol Med*. 2017;9:950–966.
33. Fan J, Shen W, Lee SR, et al. Targeting the Notch and TGF-beta signaling pathways to prevent retinal fibrosis in vitro and in vivo. *Theranostics*. 2020;10:7956–7973.
34. Zhang P, Wang H, Luo X, et al. MicroRNA-155 Inhibits Polarization of Macrophages to M2-Type and Suppresses Choroidal Neovascularization. *Inflammation*. 2018;41:143–153.
35. Zhang C, Xie H, Yang Q, et al. Erythropoietin protects outer blood-retinal barrier in experimental diabetic retinopathy by up-regulating ZO-1 and occludin. *Clin Exp Ophthalmol*. 2019;47:1182–1197.
36. Zhang J, Xu G, Zhang L, et al. A modified histoimmunochemistry-assisted method for in situ RPE evaluation. *Front Biosci (Elite Ed)*. 2012;4:1571–1581.
37. Parapuram SK, Ganti R, Hunt RC, Hunt DM. Vitreous induces components of the prostaglandin E2 pathway in human retinal pigment epithelial cells. *Invest Ophthalmol Vis Sci*. 2003;44:1767–1774.
38. Kimura K, Orita T, Fujitsu Y, et al. Inhibition by female sex hormones of collagen gel contraction mediated by retinal pigment epithelial cells. *Invest Ophthalmol Vis Sci*. 2014;55:2621–2630.
39. Espinosa-Heidmann DG, Suner I, Hernandez EP, Frazier WD, Csaky KG, Cousins SW. Age as an independent risk factor for severity of experimental choroidal neovascularization. *Invest Ophthalmol Vis Sci*. 2002;43:1567–1573.
40. Shu DY, Lovicu FJ. Myofibroblast transdifferentiation: The dark force in ocular wound healing and fibrosis. *Prog Retin Eye Res*. 2017;60:44–65.
41. Iwanishi H, Fujita N, Tomoyose K, et al. Inhibition of development of laser-induced choroidal neovascularization with suppression of infiltration of macrophages in Smad3-null mice. *Lab Invest*. 2016;96:641–651.
42. Tenbrock L, Wolf J, Boneva S, et al. Subretinal fibrosis in neovascular age-related macular degeneration: current concepts, therapeutic avenues, and future perspectives. *Cell Tissue Res*. 2022;387:361–375.
43. Shu DY, Butcher E, Saint-Geniez M. EMT and EndMT: Emerging Roles in Age-Related Macular Degeneration. *Int J Mol Sci*. 2020;21:4271.
44. Little K, Llorian-Salvador M, Tang M, et al. Macrophage to myofibroblast transition contributes to subretinal fibrosis secondary to neovascular age-related macular degeneration. *J Neuroinflammation*. 2020;17:355.
45. Mallone F, Costi R, Marenco M, et al. Understanding Drivers of Ocular Fibrosis: Current and Future Therapeutic Perspectives. *Int J Mol Sci*. 2021;22:11748.
46. De Kloe GE, De Strooper B. Small molecules that inhibit Notch signaling. *Methods Mol Biol*. 2014;1187:311–322.
47. Yang G, Zhou R, Guo X, Yan C, Lei J, Shi Y. Structural basis of gamma-secretase inhibition and modulation by small molecule drugs. *Cell*. 2021;184:521–533.e514.
48. Wong GT, Manfra D, Poulet FM, et al. Chronic treatment with the gamma-secretase inhibitor LY-411,575 inhibits beta-amyloid peptide production and alters lymphopoiesis and intestinal cell differentiation. *J Biol Chem*. 2004;279:12876–12882.
49. McKee TD, Loureiro RM, Dumin JA, Zarayskiy V, Tate B. An improved cell-based method for determining the gamma-secretase enzyme activity against both Notch and APP substrates. *J Neurosci Methods*. 2013;213:14–21.
50. Tosi GM, Caldi E, Neri G, et al. HTRA1 and TGF-beta1 Concentrations in the Aqueous Humor of Patients With Neovascular Age-Related Macular Degeneration. *Invest Ophthalmol Vis Sci*. 2017;58:162–167.
51. Tosi GM, Neri G, Caldi E, et al. Publisher Correction: TGF-beta concentrations and activity are down-regulated in the aqueous humor of patients with neovascular age-related macular degeneration. *Sci Rep*. 2018;8:10141.
52. Walshe TE, Leach LL, D'Amore PA. TGF-beta signaling is required for maintenance of retinal ganglion cell differentiation and survival. *Neuroscience*. 2011;189:123–131.
53. Braunger BM, Pielmeier S, Demmer C, et al. TGF-beta signaling protects retinal neurons from programmed cell death during the development of the mammalian eye. *J Neurosci*. 2013;33:14246–14258.
54. Braunger BM, Leimbeck SV, Schlecht A, Volz C, Jagle H, Tamm ER. Deletion of ocular transforming growth factor beta signaling mimics essential characteristics of diabetic retinopathy. *Am J Pathol*. 2015;185:1749–1768.
55. Ma W, Silverman SM, Zhao L, et al. Absence of TGFbeta signaling in retinal microglia induces retinal degeneration and exacerbates choroidal neovascularization. *Elife*. 2019;8:e42049.
56. Blokzijl A, Dahlqvist C, Reissmann E, et al. Cross-talk between the Notch and TGF-beta signaling pathways mediated by interaction of the Notch intracellular domain with Smad3. *J Cell Biol*. 2003;163:723–728.
57. Zavadil J, Cermak L, Soto-Nieves N, Bottinger EP. Integration of TGF-beta/Smad and Jagged1/Notch signalling in epithelial-to-mesenchymal transition. *EMBO J*. 2004;23:1155–1165.
58. Aimaiti Y, Yusufukadier M, Li W, et al. TGF-beta1 signaling activates hepatic stellate cells through Notch pathway. *Cytotechnology*. 2019;71:881–891.
59. Nieto MA, Huang RY, Jackson RA, Thiery JP. Emt: 2016. *Cell*. 2016;166:21–45.
60. Wu CX, Xu A, Zhang CC, et al. Notch Inhibitor PF-03084014 Inhibits Hepatocellular Carcinoma Growth and Metastasis via Suppression of Cancer Stemness due to Reduced Activation of Notch1-Stat3. *Mol Cancer Ther*. 2017;16:1531–1543.
61. Cui D, Dai J, Keller JM, Mizokami A, Xia S, Keller ET. Notch Pathway Inhibition Using PF-03084014, a gamma-Secretase

Investigative Ophthalmology & Visual Science

Inhibitor (GSI), Enhances the Antitumor Effect of Docetaxel in Prostate Cancer. *Clin Cancer Res*. 2015;21:4619–4629.

62. Maraver A, Fernandez-Marcos PJ, Herranz D, et al. Therapeutic effect of gamma-secretase inhibition in KrasG12V-driven non-small cell lung carcinoma by derepression of DUSP1 and inhibition of ERK. *Cancer Cell*. 2012;22:222–234.
63. Gridley T. Notch signaling in the vasculature. *Curr Top Dev Biol*. 2010;92:277–309.
64. Dou GR, Li N, Chang TF, et al. Myeloid-Specific Blockade of Notch Signaling Attenuates Choroidal Neovascularization through Compromised Macrophage Infiltration and Polarization in Mice. *Sci Rep*. 2016;6:28617.
65. Camelo S, Raoul W, Lavalette S, et al. Delta-like 4 inhibits choroidal neovascularization despite opposing effects on vascular endothelium and macrophages. *Angiogenesis*. 2012;15:609–622.
66. Espinosa-Heidmann DG, Suner IJ, Hernandez EP, Monroy D, Csaky KG, Cousins SW. Macrophage depletion diminishes lesion size and severity in experimental choroidal neovascularization. *Invest Ophthalmol Vis Sci*. 2003;44:3586–3592.

Investigative Ophthalmology & Visual Science